

NUCLEATION RATE CALCULATION FOR THE PHASE TRANSITION OF DIBLOCK COPOLYMERS UNDER STOCHASTIC CAHN–HILLIARD DYNAMICS*

TIEJUN LI^{†‡}, PINGWEN ZHANG[†], AND WEI ZHANG[†]

Abstract. We focus on the nucleation rate calculation for diblock copolymers by studying the two-dimensional stochastic Cahn–Hilliard dynamics with a Landau–Brazovskii energy functional. To do this, we devise the string method to compute the minimal energy path of nucleation events and the gentlest ascent dynamics to locate the saddle point on the path in Fourier space. Both methods are combined with the semi-implicit spectral method and hence are very effective. We derive the nucleation rate formula in the infinite-dimensional case and prove the convergence under numerical discretizations. The computation of the determinant ratio is also discussed for obtaining the rate. The algorithm is successfully applied to investigate the nucleation from the lamellar phase to the cylinder phase in the mean field theory for diblock copolymer melts. The comparison with projected stochastic Allen–Cahn dynamics is also discussed.

Key words. Cahn–Hilliard equation, diblock copolymer, Landau–Brazovskii energy, string method, nucleation rate, functional determinant ratio

AMS subject classification. 65C20

DOI. 10.1137/120876307

1. Introduction. In the past few decades, diblock copolymers [22, 12] have been extensively investigated due to their interesting physical and chemical features as well as widespread applications in material science [13, 6]. Roughly speaking, the studies of copolymers mainly focus on two kinds of issues: determining equilibrium phases and studying the dynamical behaviors. For the first issue, it has been known for a long time that the diblock copolymers admit various ordered phase separation in the microscale. Several kinds of stable ordered phases, such as the lamellar phase, cylinder phase, and spherical phase, etc., have been discovered in experiments, and lots of work has been done to determine the phase diagram [33, 23]. For the second issue, people try to understand the dynamical behaviors of the diblock copolymers, for example, the interfacial motion [19, 24], spinodal decomposition phenomena [28], and nucleation events between different kinds of ordered phases [31, 21, 5].

In this paper, we study the nucleation rate calculation for diblock copolymers between the lamellar and cylinder phases with a Landau–Brazovskii energy functional, and the random fluctuation is assumed to be of stochastic Cahn–Hilliard type. In this model, it is supposed that diblock copolymer melts contain lots of chains, each of which contains monomers of types A and B linked together (see Figure 1.1). On each chain, the composition ratios of these two kinds of monomers are f_A and f_B , respectively, which satisfy $f_A + f_B = 1$. The order parameters $\phi_A(\mathbf{r})$ and $\phi_B(\mathbf{r})$ characterize

*Received by the editors May 7, 2012; accepted for publication (in revised form) January 30, 2013; published electronically March 21, 2013.

<http://www.siam.org/journals/mms/11-1/87630.html>

[†]Laboratory of Mathematics and Applied Mathematics (LMAM) and School of Mathematical Sciences, Peking University, Beijing 100871, People’s Republic of China (tieli@pku.edu.cn, pzhang@pku.edu.cn, wzhangpku@gmail.com). The first author’s research was supported by the NSFC under grants 11171009 and 91130005. The second author’s research was supported by the NSFC under grant 50930003.

[‡]Beijing International Center for Mathematical Research (BICMR), Beijing 100871, People’s Republic of China.

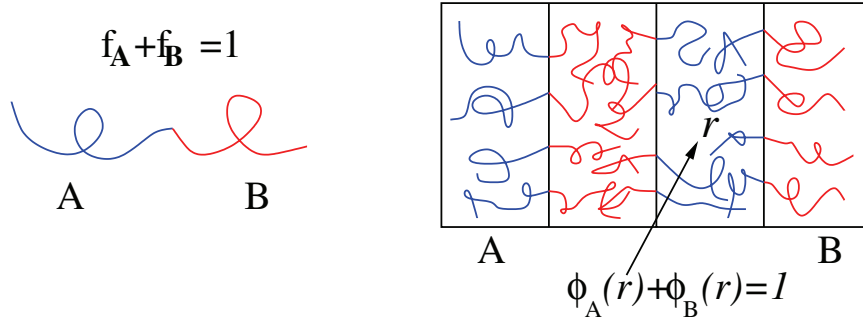


FIG. 1.1. *Left part: Single diblock copolymer with components A and B and the composition ratio f_A and f_B . Right part: The field description of diblock polymer melts in the lamellar phase. The volume fractions $\phi_A(\mathbf{r})$ and $\phi_B(\mathbf{r})$ are defined for components A and B at each point \mathbf{r} in space.*

the volume fractions of A and B in physical space, and therefore $\phi_A(\mathbf{r}) + \phi_B(\mathbf{r}) \equiv 1$. Letting $\phi(\mathbf{r}) = \phi_A(\mathbf{r}) - f_A$ and Ω being the physical domain, $\phi(\mathbf{r})$ satisfies the conservation law $\int_{\Omega} \phi(\mathbf{r}) \, d\mathbf{r} = 0$. The Landau–Brazovskii energy functional [33, 31] for order parameter ϕ is defined as

$$(1.1) \quad \mathcal{F}(\phi) = \int_{\Omega} \left\{ \frac{\xi^2}{2} [(\Delta + 1)\phi(\mathbf{r})]^2 + \Phi(\phi) \right\} d\mathbf{r},$$

where

$$(1.2) \quad \Phi(\phi) = \frac{\tau}{2}\phi^2 - \frac{\gamma}{3!}\phi^3 + \frac{1}{4!}\phi^4,$$

and ξ, γ, τ are constant parameters of the system. Since ϕ is conservative, one commonly used assumption on its dynamics is that it satisfies the following Cahn–Hilliard equation (also known as Model B in condensed matter physics [3, 17]):

$$(1.3) \quad \frac{\partial \phi}{\partial t} = \Delta \frac{\delta \mathcal{F}}{\delta \phi} = \Delta \left[\xi^2 (\Delta + 1)^2 \phi + \Phi_1(\phi) \right],$$

with $\Phi_1(\phi) = \Phi'(\phi) = \tau\phi - \gamma\phi^2/2! + \phi^3/3!$. When taking the noise's effects into consideration, we need also consider the corresponding stochastic Cahn–Hilliard equation

$$(1.4) \quad \frac{\partial \phi}{\partial t} = \Delta \frac{\delta \mathcal{F}}{\delta \phi} + \sqrt{2\epsilon} \xi,$$

where the noise ξ has the correlation $E(\xi(\mathbf{x}, t)\xi(\mathbf{y}, s)) = -\Delta\delta(\mathbf{x} - \mathbf{y})\delta(t - s)$, and ϵ is the noise intensity.

From the perspective of rare events [9], equation (1.4) is a typical infinite-dimensional deterministic system perturbed by small noise. It is expected that the metastability will appear in the transitions between the metastable states. In the present work, we consider the two-dimensional (2D) case with periodic boundary conditions (BCs), derive the nucleation rate formula of the system, and aim to develop efficient numerical methods to study the nucleation rate. Along this way, the string method to locate the minimal energy path (MEP) and the method to find the saddle point precisely are devised in Fourier space. As an application, we consider the transition between the lamellar phase to the cylinder phase of system (1.4), and the algorithm

can be easily applied to the transitions between other metastable states. This work is based on our previous study on the one-dimensional (1D) stochastic Cahn–Hilliard equation [34]. The main contributions of this paper are as follows:

- We devise the string method along the lines in [7, 8] to locate the MEP, which is also the most probable transition path, for the stochastic Cahn–Hilliard dynamics (1.4). It is characterized by the fact that Cahn–Hilliard dynamics is indeed a gradient flow in H^{-1} space. More concretely, the MEP u^* is described by the concatenation of two parts

$$(1.5) \quad \lim_{t \rightarrow -\infty} u^*(t) = a, \quad \lim_{t \rightarrow +\infty} u^*(t) = c, \quad \frac{\partial u^*}{\partial t} = -\Delta \frac{\delta F}{\delta u}$$

and

$$(1.6) \quad \lim_{t \rightarrow -\infty} u^*(t) = c, \quad \lim_{t \rightarrow +\infty} u^*(t) = b, \quad \frac{\partial u^*}{\partial t} = \Delta \frac{\delta F}{\delta u},$$

where a, b are metastable states we are interested in, and c is a connecting saddle point between them. The MEP can be obtained by evolving the string connecting the metastable states until it achieves equilibrium. In the present paper, all of the implementations are combined with the spectral formulation of the equation, which leads to efficient and accurate treatment for higher order differentials.

- We discuss the gentlest ascent dynamics (GAD) [10] to locate the saddle point based on a rough estimate from the MEP by the string method within the framework of the spectral method. The exact location of the saddle point is very important for computing the nucleation rate and has been discussed in literatures with both theoretical [20] and numerical [14, 15, 10, 32, 16] methods. Our approach is superior to the climbing image method utilized before [15, 8], and it is a perfect setup to adopt the local convergence property of GAD with an available good initial guess.
- We derive the nucleation formula for system (1.4) and establish a convergence theorem for computing the nucleation rate. By asymptotic analysis [34], the nucleation rate can be given, which includes a ratio

$$(1.7) \quad R_k^\infty = \prod_{j=k}^{+\infty} \lambda_j^a / \lambda_j^c,$$

where k is fixed, and λ_j^a, λ_j^c are eigenvalues of the Hessian operators of the Landau–Brazovskii energy functional at states a and c . In numerics, we should take finite-dimensional approximation. It is well known that the approximations to large eigenvalues with a given resolution become inaccurate [29]. But we can show that the convergence of the ratio to its infinite-dimensional counterpart still holds by taking the special feature of the problem as the discretization goes to infinity. We think this result is fundamental for the nucleation rate calculation in infinite dimensions.

- We compare the differences between stochastic Cahn–Hilliard dynamics (1.4) with the projected Allen–Cahn dynamics [21, 11], which can also be used to describe the evolution of conservative order parameters. While these two dynamics share the same metastable states and saddle points, the MEPs and the nucleation rates are essentially different. We investigate the differences between these two models through asymptotic analysis and numerical results.

Besides the above points, we also discuss the algorithms for computing the determinant ratio in finite dimensions, which is not straightforward when the system size is very large. They are also meaningful for further investigations.

The organization of this paper is as follows. In section 2, we consider the concrete model setup and the Galerkin discretization of the stochastic Cahn–Hilliard equation (1.4), which leads to stochastic differential equations in the Fourier space. In section 3, we design the string method to find the MEP and the GAD method to locate the saddle point on the path in Fourier space. In section 4, we give the nucleation rate formula and discuss algorithms to compute the nucleation rate of the discretized system and the original system (1.4). In section 5, we compare the differences of the MEPs and the nucleation rates for the stochastic Cahn–Hilliard dynamics (1.4) with the projected Allen–Cahn dynamics. In section 6, we apply our algorithms to study the nucleation event between the lamellar and cylinder phases for diblock copolymers. Further discussions and possible extensions are included in section 7. In section 8, we make conclusions. The detailed derivation of Galerkin discretization for (1.4) is given in Appendix A. The convergence of the determinant ratio is proved in Appendix B.

2. Model setup. In this section, we consider the precise mathematical setup and the spectral discretization for stochastic Cahn–Hilliard equation (1.4), which is needed in later sections. More detailed derivations and specific notations can be found in Appendix A.

In two dimensions, we assume the physical domain is $\Omega = [0, L_x] \times [0, L_y]$, with periodic BC and $V = |\Omega|$. We introduce the spaces

$$(2.1) \quad \begin{aligned} L_{per}^2(\Omega) &= \left\{ \phi(\mathbf{r}) \mid \phi(\mathbf{r}) \text{ is periodic} \right\}, \\ L_{per,0}^2(\Omega) &= L_{per}^2(\Omega) \cap \left\{ \phi(\mathbf{r}) \mid \frac{1}{V} \int_{\Omega} \phi(\mathbf{r}) \, d\mathbf{r} = 0 \right\}, \end{aligned}$$

and the orthogonal projection operator $\mathcal{P} : L_{per}^2(\Omega) \rightarrow L_{per,0}^2(\Omega)$ is defined by $\mathcal{P}\phi = \phi - \frac{1}{V} \int_{\Omega} \phi(\mathbf{r}) \, d\mathbf{r} \, \forall \phi \in L_{per}^2(\Omega)$. With the indices sets

$$(2.2) \quad \begin{aligned} \mathcal{I} &= \left\{ (k, l) \mid k, l \in \mathbb{Z}, (k, l) \neq (0, 0) \right\}, \\ \mathcal{I}_r &= \left\{ (k, l) \mid k, l \geq 0, k, l \in \mathbb{Z}, (k, l) \neq (0, 0) \right\} \cup \left\{ (k, l) \mid k < 0, l \geq 1, k, l \in \mathbb{Z} \right\}, \end{aligned}$$

the basis functions of $L_{per,0}^2(\Omega)$ are

$$(2.3) \quad e_{\mathbf{j}}(x, y) = e^{2\pi i \left(\frac{kx}{L_x} + \frac{ly}{L_y} \right)} \quad \forall \mathbf{j} = (k, l) \in \mathcal{I},$$

with complex form, and

$$(2.4) \quad \begin{aligned} e_{j,1}(x, y) &= \sqrt{2} \cos \left(2\pi \left(\frac{kx}{L_x} + \frac{ly}{L_y} \right) \right) \quad \forall \mathbf{j} = (k, l) \in \mathcal{I}_r, \\ e_{j,2}(x, y) &= \sqrt{2} \sin \left(2\pi \left(\frac{kx}{L_x} + \frac{ly}{L_y} \right) \right) \quad \forall \mathbf{j} = (k, l) \in \mathcal{I}_r, \end{aligned}$$

with real form.

To make (1.4) more precise, we rewrite it with the notations in stochastic analysis as

$$(2.5) \quad d\phi(t) = \Delta \frac{\delta \mathcal{F}}{\delta \phi} dt + \sqrt{2\epsilon} dW(t),$$

and $W(t)$ is the cylindrical Q-Wiener process which can be expressed as

$$(2.6) \quad W(t) = \sum_{j \in \mathcal{I}} \sqrt{\rho_j} W_j(t) e_j = \sum_{j \in \mathcal{I}_r} \sqrt{\rho_j} (W_{j,1}(t) e_{j,1} + W_{j,2}(t) e_{j,2}),$$

where $\rho_j = (2\pi k/L_x)^2 + (2\pi l/L_y)^2$ corresponds to the eigenvalues of the covariance operator $Q = -\Delta$. The complex Brownian motion is defined as

$$(2.7) \quad W_j(t) = \frac{1}{\sqrt{2}} (W_{j,1}(t) - iW_{j,2}(t)),$$

where $W_{j,1}(t), W_{j,2}(t)$ are independent real Brownian motions. $W_j(t)$ satisfies $W_{-j}(t) = \overline{W_j(t)} \forall j = (k, l) \in \mathcal{I}$ (with this type of noise, we are considering the fluctuations on the flux and the solution of (1.4) is conservative; see Remark 2.1 in [34]).

For notational convenience, we introduce the operators

$$(2.8) \quad \mathcal{L}_1(\phi) = \mathcal{P} \frac{\delta \mathcal{F}}{\delta \phi} = \xi^2 (\Delta + 1)^2 \phi + \mathcal{P} \Phi_1(\phi),$$

$$(2.9) \quad \mathcal{L}_2(\phi)\psi = \mathcal{P} \frac{\delta^2 \mathcal{F}}{\delta \phi^2}(\phi)\psi = \xi^2 (\Delta + 1)^2 \psi + \mathcal{P}(\Phi_2(\phi)\psi),$$

where $\Phi_2(\phi) = \Phi''(\phi) = \tau - \gamma\phi + \frac{1}{2}\phi^2$. Denoting $n_1, n_2 \in \mathbb{N}^+$, $\mathbf{n} = (n_1, n_2)$, we introduce index subsets $\mathcal{I}_{\mathbf{n}}, \mathcal{I}_{r,\mathbf{n}}$, complex subspace $\mathcal{S}_{\mathbf{n}} = \text{span}\{e_j, j \in \mathcal{I}_{\mathbf{n}}\}$, real subspace $\mathcal{S}_{r,\mathbf{n}} = \text{span}\{e_{j,1}, e_{j,2}, j \in \mathcal{I}_{r,\mathbf{n}}\}$, and projection operators $\mathcal{P}_{\mathbf{n}}, \mathcal{P}_{r,\mathbf{n}}$ on subspaces $\mathcal{S}_{\mathbf{n}}, \mathcal{S}_{r,\mathbf{n}}$ (see Appendix A for more specific forms).

On subspace $\mathcal{S}_{\mathbf{n}}$, the Galerkin method for stochastic Cahn–Hilliard equation (1.4) is to find $\phi(\cdot, t) = \sum_{j \in \mathcal{I}_{\mathbf{n}}} \phi_j(t) e_j \in \mathcal{S}_{\mathbf{n}}$ such that

$$(2.10) \quad \langle d\phi(\cdot, t) - \Delta \mathcal{L}_1(\phi(\cdot, t)) dt, e_j \rangle = \langle \sqrt{2\epsilon} dW, e_j \rangle \quad \forall j \in \mathcal{I}_{\mathbf{n}},$$

which leads to stochastic differential equations

$$(2.11) \quad d\phi_j(t) = -\rho_j [\xi^2 (1 - \rho_j)^2 \phi_j(t) + Q_j(t)] dt + \sqrt{2\epsilon \rho_j} dW_j(t), \quad j \in \mathcal{I}_{\mathbf{n}},$$

with nonlinear terms

$$(2.12) \quad Q_j(t) = \langle \Phi_1(\phi), e_j \rangle = \tau \phi_j(t) - \frac{\gamma}{2!} \sum_{\substack{\mathbf{p}+\mathbf{q}=\mathbf{j} \\ \mathbf{p}, \mathbf{q} \in \mathcal{I}_{\mathbf{n}}}} \phi_{\mathbf{p}}(t) \phi_{\mathbf{q}}(t) + \frac{1}{3!} \sum_{\substack{\mathbf{p}+\mathbf{q}+\mathbf{r}=\mathbf{j} \\ \mathbf{p}, \mathbf{q}, \mathbf{r} \in \mathcal{I}_{\mathbf{n}}}} \phi_{\mathbf{p}}(t) \phi_{\mathbf{q}}(t) \phi_{\mathbf{r}}(t).$$

On subspace $\mathcal{S}_{r,\mathbf{n}}$, the Galerkin method for (1.4) is to find

$$\phi^r(\cdot, t) = \sum_{j \in \mathcal{I}_{r,\mathbf{n}}} (a_j(t) e_{j,1} + b_j(t) e_{j,2}) \in \mathcal{S}_{r,\mathbf{n}},$$

which solves

$$(2.13) \quad \langle d\phi^r(\cdot, t) - \Delta \mathcal{L}_1(\phi^r(\cdot, t)) dt, e_{j,l} \rangle = \langle \sqrt{2\epsilon} dW(t), e_{j,l} \rangle = \sqrt{2\epsilon \rho_j} dW_{j,l}(t), \\ l = 1, 2, \forall j \in \mathcal{I}_{r,\mathbf{n}}.$$

Let $\#\mathcal{I}_{r,n} = n_r$ and $n = 2n_r$. After ordering the indices in $\mathcal{I}_{r,n}$, coefficients $a_j(t), b_j(t)$, basis functions $e_{j,1}, e_{j,2}$, ρ_j , and Brownian motions $W_{j,1}, W_{j,2}$ can be written as $\mathbf{x}, \boldsymbol{\omega}, D, W$, which are vectors of length n . Then (2.13) is equivalent to

$$(2.14) \quad dx_l = -D_l \langle \mathcal{L}_1(\phi^r), \omega_l \rangle dt + \sqrt{2\epsilon D_l} dW_l, \quad l = 1, 2, \dots, n.$$

Let $F_r(\mathbf{x}) = \mathcal{F}(\phi^r)/V$, $\phi^r = \sum_{l=1}^n x_l \omega_l$. With the notations

$$G = \text{diag}\{D_1, D_2, \dots, D_n\}, \quad \nabla F_r = \left(\frac{\partial F_r}{\partial x_1}, \frac{\partial F_r}{\partial x_2}, \dots, \frac{\partial F_r}{\partial x_n} \right)^T,$$

(2.14) can be reformulated as a generalized stochastic gradient system in \mathbb{R}^n :

$$(2.15) \quad d\mathbf{x} = -G \nabla F_r dt + \sqrt{2\epsilon} G^{\frac{1}{2}} dW.$$

The Galerkin method on \mathcal{S}_n , which leads to (2.11), is equivalent to the Galerkin method on $\mathcal{S}_{r,n}$ with (2.15). Equation (2.11) is more specific and suitable for designing and implementing algorithms, while (2.15) has the form of a generalized stochastic gradient system, indicating the possibility of the string method which will be discussed below. The Galerkin discretization of the deterministic Cahn–Hilliard equation (1.3) could be obtained in the same way by dropping the stochastic terms, and we have

$$(2.16) \quad \frac{d\phi_j(t)}{dt} = -\rho_j \langle \mathcal{L}_1(\phi^c(\cdot, t)), e_j \rangle = -\rho_j \left[\xi^2 (1 - \rho_j)^2 \phi_j(t) + Q_j(t) \right], \quad \mathbf{j} \in \mathcal{I}_n,$$

and

$$(2.17) \quad \frac{d\mathbf{x}}{dt} = -G \nabla F_r.$$

Remark 1. For comparison, we briefly write down the discretization formulation with the finite difference approximation method for the evolution equation (1.3). Given $N_x, N_y \in \mathbb{Z}$, let $\Delta x = L_x/N_x$, $\Delta y = L_y/N_y$, $x_i = (i + \frac{1}{2})\Delta x$, $i = 0, 1, \dots, N_x - 1$, $y_j = (j + \frac{1}{2})\Delta y$, $j = 0, 1, \dots, N_y - 1$. We use two subscripts to represent vectors and identify subscripts $(i, -1)$ with $(i, N_y - 1)$ and also $(-1, j)$ with $(N_x - 1, j)$. Let $\phi_{i,j} = \phi(x_i, y_j)$, i.e., the value of ϕ at each grid center, and let D denote the second order centered finite difference approximation of the Laplacian operator $-\Delta$ with periodic BC. For energy functional \mathcal{F} in (1.1), the term $(\Delta + 1)\phi$ is discretized to P , with components

$$P_{i,j} = \frac{\phi_{i+1,j} + \phi_{i-1,j} - 2\phi_{i,j}}{\Delta x^2} + \frac{\phi_{i,j+1} + \phi_{i,j-1} - 2\phi_{i,j}}{\Delta y^2} + \phi_{i,j}.$$

We also reuse the notation ϕ as the discrete vector. Therefore \mathcal{F} can be discretized as

$$(2.18) \quad F[\phi] = \frac{1}{V} \sum_{i=0}^{N_x-1} \sum_{j=0}^{N_y-1} \left[\frac{\xi^2}{2} P_{i,j}^2 + \frac{\tau}{2} \phi_{i,j}^2 - \frac{\gamma}{3!} \phi_{i,j}^3 + \frac{1}{4!} \phi_{i,j}^4 \right] \Delta x \Delta y,$$

with gradient

$$(\nabla F)_{i,j} = \frac{\partial F}{\partial \phi_{i,j}} = \frac{\Delta x \Delta y}{V} \sum_{k=0}^{N_x-1} \sum_{l=0}^{N_y-1} \left[\xi^2 P_{k,l} \frac{\partial P_{k,l}}{\partial \phi_{i,j}} + \left(\tau \phi_{k,l} - \frac{\gamma}{2} \phi_{k,l}^2 + \frac{1}{3!} \phi_{k,l}^3 \right) \delta_{k,i} \delta_{l,j} \right].$$

Then the discretized version of evolution equation (1.3) could be written as

$$(2.19) \quad \frac{d\phi}{dt} = -D \nabla F,$$

which is also a generalized gradient system.

3. Metastable phases, saddle point, and MEP. In this section, based on the spectral discretization (2.11) and (2.14), we will study numerical methods for nucleation events of system (1.4).

3.1. Numerical methods for MEP and saddle point. For simplicity, we focus on the nucleation event from the lamellar phase to the cylinder phase. In two dimensions and with appropriate parameters τ, ξ, γ , lamellar and cylinder phases are two kinds of ordered metastable phases whose order parameters are both local minimizers of Landau–Brazovskii energy functional (1.1) and stable states of dynamical system (1.3). With (2.16), these states can be computed using semi-implicit spectral method [4] with suitable initial values (for example, single mode approximation [31]):

$$(3.1) \quad \left[1 + \xi^2 \Delta t \rho_j (1 - \rho_j)^2\right] \phi_j^{k+1} = \phi_j^k - \Delta t \rho_j Q_j^k, \quad \mathbf{j} \in \mathcal{I}_n, \quad k = 0, 1, 2, \dots,$$

where Δt is the time step size, and Q_j^k follows (2.12). Now consider the nucleation event of the generalized stochastic gradient system (2.14) between two local minima a (lamellar phase) and b (cylinder phase). Let $\Omega(a)$ and $\Omega(b)$ denote the attractive basins of states a and b under dynamical system (1.3), respectively. The MEP $u^*(\cdot, t) \in \mathbb{R}^n$, which is the most probable transition path from a to b in zero temperature limit, is described by the concatenation of two parts

$$(3.2) \quad \lim_{t \rightarrow -\infty} u^*(t) = a, \quad \lim_{t \rightarrow +\infty} u^*(t) = c, \quad \frac{du^*}{dt} = G \nabla F_r$$

and

$$(3.3) \quad \lim_{t \rightarrow -\infty} u^*(t) = c, \quad \lim_{t \rightarrow +\infty} u^*(t) = b, \quad \frac{du^*}{dt} = -G \nabla F_r,$$

where $c \in \partial\Omega(a) \cap \partial\Omega(b)$ is the saddle point. Intuitively, starting from the metastable state a , the MEP will follow the steepest ascent dynamics (3.2), arrive at the saddle point when crossing $\partial\Omega(a)$, and then follow the steepest descent dynamics (3.3) until it reaches the other metastable state b .

To solve MEP (3.2), (3.3), we propose the string method along the lines in [7]. That is, consider $\mathbf{z}(s) = \mathbf{x}(\cdot, s) \in \mathbb{R}^n$ as a continuous path in the space of Fourier coefficients, $s \in [0, 1]$ being the arc-length parameter. $\mathbf{z}(0), \mathbf{z}(1)$ locate in $\Omega(a)$ and $\Omega(b)$, respectively. Discretizing $\mathbf{z}(s)$, we obtain nodes $\mathbf{z}_1, \mathbf{z}_2, \dots, \mathbf{z}_N \in \mathbb{R}^n$ to describe the MEP. Algorithm 1 illustrates the string method to solve the MEP (3.2), (3.3) connecting metastable states a, b . Here we would like to emphasize that while spectral discretization is used to approximate each node on the transition path, linear interpolation is used to redistribute the discrete nodes on the continuous transition path in path space. These two methods are applied in two different spaces (one is the function space of all possible phases and the other is the path space) and thus are independent in some sense. We could expect order one precision for the whole transition path but still spectral precision for each node. More precise approximation for the transition path could be obtained by increasing the number of discrete nodes which represent the path, by a higher order interpolation method, or by using a weighted distance function in the reparameterization procedure of the string method [8]. In our work, the precise location of the saddle point on the transition path is further obtained by the GAD method discussed below.

In the following, $\mathbf{x}^a, \mathbf{x}^b, \mathbf{x}^c$ denote the Fourier coefficients of states a, b, c , respectively, and H^a, H^c are the Hessian matrices of F_r at \mathbf{x}^a and \mathbf{x}^c .

Algorithm 1: String method of stochastic generalized gradient system (2.15)

- 1 Initialization. At $k = 0$, use the single mode approximation of the ordered phases a and b to initialize \mathbf{z}_1^0 and \mathbf{z}_N^0 and compute $\mathbf{z}_l^0, l = 2, 3, \dots, N - 1$, by linearly interpolating \mathbf{z}_1^0 and \mathbf{z}_N^0 .
 - 2 Update. At the k th step, update each discretized nodes \mathbf{z}_l^k using semi-implicit spectral method (3.1) and obtain $\mathbf{z}_l^{k+\frac{1}{2}}, l = 1, 2, \dots, N$.
 - 3 Reparameterization. Linearly interpolate the updated nodes $\mathbf{z}_l^{k+\frac{1}{2}}$, and obtain \mathbf{z}_l^{k+1} at the $(k + 1)$ st step, $l = 1, 2, \dots, N$.
 - 4 Iterate the above two steps until the nodes converge.
-

For $\mathbf{u}, \mathbf{v} \in \mathbb{R}^n$, let $\langle \mathbf{u}, \mathbf{v} \rangle_G = \mathbf{u}^T G^{-1} \mathbf{v}$. System (2.17) becomes a gradient system under $\langle \cdot, \cdot \rangle_G$, and the gradient of F_r is $G \nabla F_r$. State c is the critical state along the MEP and is also index-1 saddle point of dynamical system (2.17). Following [10], it could be computed by the GAD method:

$$(3.4) \quad \begin{cases} \dot{\mathbf{x}} = -G \nabla F_r(\mathbf{x}) + 2 \frac{\mathbf{v}^T \nabla F_r(\mathbf{x})}{\mathbf{v}^T G^{-1} \mathbf{v}} \mathbf{v}, \\ \dot{\mathbf{v}} = -G \nabla^2 F_r(\mathbf{x}) \mathbf{v} + \frac{\mathbf{v}^T \nabla^2 F_r(\mathbf{x}) \mathbf{v}}{\mathbf{v}^T G^{-1} \mathbf{v}} \mathbf{v}, \end{cases}$$

with a good initial guess from the result given by the string method. In (3.4), we need to compute the product of the Hessian matrix of F_r with vector $\mathbf{v} \in \mathbb{R}^n$. Denoting $\nabla^2 F_r(\mathbf{x}) = (H_{kl}), 1 \leq k, l \leq n, \mathbf{x} = (x_1, x_2, \dots, x_n)^T, \phi^r = \sum_{l=1}^n x_l \omega_l$, it follows that

$$(3.5) \quad H_{kl} = \frac{\partial^2 F_r}{\partial x_k \partial x_l} = \langle \mathcal{L}_2(\phi^r) \omega_l, \omega_k \rangle$$

$\forall \mathbf{v} = (v_1, v_2, \dots, v_n)^T \in \mathbb{R}^n, (H\mathbf{v})_k = \sum_{l=1}^n H_{kl} v_l = \langle \mathcal{L}_2(\phi^r) \sum_{l=1}^n v_l \omega_l, \omega_k \rangle$. Letting $\psi_{\mathbf{v}} = \sum_{l=1}^n v_l \omega_l$, the above derivation shows that the components $(H\mathbf{v})_k$ of the product $H\mathbf{v}$ are just the real and imaginary parts of the Fourier coefficients of $\mathcal{L}_2(\phi^r) \psi_{\mathbf{v}}$. Numerically, the Fourier coefficients of $\mathcal{L}_1(\phi^r)$ and $\mathcal{L}_2(\phi^r) \psi_{\mathbf{v}}$ are computed by first converting into real space to handle the convolution terms in (2.12) and then converting back to Fourier space using FFT. Notice that the semi-implicit spectral method, which is similar to (3.1), can still be used when computing the saddle point with (3.4). After the convergence of (3.4), we could obtain the Fourier coefficients \mathbf{x}^c of the saddle point c , as well as the eigenvector $\tilde{\mathbf{v}}_1$ of matrix GH^c corresponding to the negative eigenvalue $\mu_{1,n}$, which is unique.

3.2. Degeneracy of metastable states and saddle points. The order parameters with respect to metastable state a and saddle point c are $\phi^a(x, y) = \sum_{l=1}^n x_l^a \omega_l$ and $\phi^c(x, y) = \sum_{l=1}^n x_l^c \omega_l$. Under periodic BC, assume the orientation of the lamellar phase is along the x -direction; then $\phi^a(x, y)$ is constant for given y . Since the energy functional (1.1) is invariant under translations, it follows that

$$\mathcal{L}_1(\phi^a(x, y + \theta_1)) = 0, \quad \mathcal{L}_1(\phi^c(x + \theta_2, y + \theta_3)) = 0 \quad \forall \theta_1, \theta_2, \theta_3 \in \mathbb{R}.$$

Taking derivatives with respect to $\theta_1, \theta_2, \theta_3$, we obtain

$$(3.6) \quad \mathcal{L}_2(\phi^a) \left(\frac{\partial}{\partial y} \phi^a(x, y) \right) = 0, \quad \mathcal{L}_2(\phi^c) \left(\frac{\partial}{\partial x} \phi^c(x, y) \right) = 0, \quad \mathcal{L}_2(\phi^c) \left(\frac{\partial}{\partial y} \phi^c(x, y) \right) = 0,$$

which indicates that the Hessian matrices H^a, H^c have an eigenvalue zero. Let

$$(3.7) \quad \zeta^x = (\zeta_1^x, \zeta_2^x, \dots, \zeta_n^x)^T, \quad \zeta^y = (\zeta_1^y, \zeta_2^y, \dots, \zeta_n^y)^T,$$

where for $j_l = (j_l, k_l) \in \mathcal{I}_{r,n}$, $l = 1, 2, \dots, n_r$,

$$(3.8) \quad \zeta_l^x = \frac{2\pi j_l}{L_x}, \quad \zeta_{l+n_r}^x = -\frac{2\pi j_l}{L_x}, \quad \zeta_l^y = \frac{2\pi k_l}{L_y}, \quad \zeta_{l+n_r}^y = -\frac{2\pi k_l}{L_y}.$$

Then we have $\frac{\partial}{\partial y} \phi^a(x, y) = \sum_{l=1}^n \zeta_l^y x_{\sigma(l)}^a \omega_l$, where $1 \leq \sigma(l) \leq n$, $|\sigma(l) - l| = n_r$. We could parameterize the Fourier coefficients of metastable states

$$\mathbf{x}^a(\theta_1) = (x_1^a(\theta_1), x_2^a(\theta_1), \dots, x_n^a(\theta_1))^T, \quad \theta_1 \in [0, L_y],$$

with

$$(3.9) \quad \begin{aligned} x_l^a(\theta_1) &= x_l^a \cos(\zeta_l^y \theta_1) + x_{l+n_r}^a \sin(\zeta_l^y \theta_1), \\ x_{l+n_r}^a(\theta_1) &= -x_l^a \sin(\zeta_l^y \theta_1) + x_{l+n_r}^a \cos(\zeta_l^y \theta_1), \end{aligned}$$

where $l = 1, 2, \dots, n_r$, and also for the saddle points

$$\mathbf{x}^c(\theta_2, \theta_3) = (x_1^c(\theta_2, \theta_3), x_2^c(\theta_2, \theta_3), \dots, x_n^c(\theta_2, \theta_3))^T, \quad \theta_2 \in [0, L_x], \theta_3 \in [0, L_y],$$

with

$$(3.10) \quad \begin{aligned} x_l^c(\theta_2, \theta_3) &= x_l^c \cos(\zeta_l^x \theta_2 + \zeta_l^y \theta_3) + x_{l+n_r}^c \sin(\zeta_l^x \theta_2 + \zeta_l^y \theta_3), \\ x_{l+n_r}^c(\theta_2, \theta_3) &= -x_l^c \sin(\zeta_l^x \theta_2 + \zeta_l^y \theta_3) + x_{l+n_r}^c \cos(\zeta_l^x \theta_2 + \zeta_l^y \theta_3), \end{aligned}$$

where $l = 1, 2, \dots, n_r$. Thus the eigenvector of H^a corresponding to eigenvalue zero is

$$(3.11) \quad (\zeta_1^y x_{\sigma(1)}^a, \zeta_2^y x_{\sigma(2)}^a, \dots, \zeta_n^y x_{\sigma(n)}^a)^T.$$

Similarly, H^c has two eigenvectors corresponding to eigenvalue zero, which are

$$(3.12) \quad (\zeta_1^x x_{\sigma(1)}^c, \zeta_2^x x_{\sigma(2)}^c, \dots, \zeta_n^x x_{\sigma(n)}^c)^T, \quad (\zeta_1^y x_{\sigma(1)}^c, \zeta_2^y x_{\sigma(2)}^c, \dots, \zeta_n^y x_{\sigma(n)}^c)^T.$$

After normalization and orthogonalization, we could obtain orthonormal eigenvectors \mathbf{v}_1^a and $\mathbf{v}_2^c, \mathbf{v}_3^c$.

4. Nucleation rate.

4.1. Nucleation rate formula. In the previous section, we demonstrated the degeneracy of the metastable states and saddle points under periodic BC. From (3.9), (3.10), it is straightforward to check that

$$(4.1) \quad \|\nabla \mathbf{x}^a(\theta_1)\|_2 = \left(\sum_{l=1}^n (\zeta_l^y x_{\sigma(l)}^a)^2 \right)^{\frac{1}{2}},$$

$$(4.2) \quad \begin{aligned} & \sqrt{\det(\nabla \mathbf{x}^c(\theta_2, \theta_3) (\nabla \mathbf{x}^c(\theta_2, \theta_3)))^T} \\ &= \left[\sum_{l=1}^n (\zeta_l^x x_{\sigma(l)}^c)^2 \sum_{l=1}^n (\zeta_l^y x_{\sigma(l)}^c)^2 - \left(\sum_{l=1}^n \zeta_l^x \zeta_l^y (x_{\sigma(l)}^c)^2 \right)^2 \right]^{\frac{1}{2}}; \end{aligned}$$

thus they are independent of the parameters $\theta_2 \in [0, L_x]$, $\theta_1, \theta_3 \in [0, L_y]$ and can be denoted by Λ_n^a, Λ_n^c , respectively. With these notations, the nucleation rate formula of system (2.15) can be derived following [34, 30] as (also see [27])

$$(4.3) \quad k_n = \frac{|\mu_{1,n}|}{2\pi} (2\pi\epsilon)^{-\frac{1}{2}} \sqrt{\frac{\tilde{\det}H^a}{|\tilde{\det}H^c|}} \frac{L_x \Lambda_n^c}{\Lambda_n^a} e^{-\frac{\Delta F_r}{\epsilon}},$$

where $\tilde{\det}H$ denotes the product of all the nonzero eigenvalues of matrix H . Denote the eigenvalues of matrices H^a and H^c by $\lambda_{j,n}^a, \lambda_{j,n}^c, j = 1, 2, \dots, n$; then (4.3) can be represented using these eigenvalues as

$$(4.4) \quad k_n = \frac{|\mu_{1,n}|}{2\pi} (2\pi\epsilon)^{-\frac{1}{2}} \left(\frac{\lambda_{2,n}^a \lambda_{3,n}^a}{|\lambda_{1,n}^c|} \right)^{\frac{1}{2}} \left(\prod_{j=4}^n \lambda_{j,n}^a / \lambda_{j,n}^c \right)^{\frac{1}{2}} \frac{L_x \Lambda_n^c}{\Lambda_n^a} e^{-\frac{\Delta F_r}{\epsilon}},$$

where $0 = \lambda_{1,n}^a < \lambda_{2,n}^a \leq \lambda_{3,n}^a \leq \dots \leq \lambda_{n,n}^a$, and $\lambda_{1,n}^c < 0 = \lambda_{2,n}^c = \lambda_{3,n}^c < \lambda_{4,n}^c \leq \dots \leq \lambda_{n,n}^c$.

Intuitively, letting $n \rightarrow +\infty$, we obtain the nucleation rate formula for stochastic Cahn–Hilliard equation (1.4) with periodic BC:

$$(4.5) \quad k = \frac{|\mu|}{2\pi} (2\pi\epsilon)^{-\frac{1}{2}} \left(\frac{\lambda_2^a \lambda_3^a}{|\lambda_1^c|} \right)^{\frac{1}{2}} \left(\prod_{j=4}^{+\infty} \lambda_j^a / \lambda_j^c \right)^{\frac{1}{2}} \frac{L_x \Lambda^c}{\Lambda^a} e^{-\frac{\Delta F_r}{\epsilon}},$$

where Λ^a, Λ^c are the infinite-dimensional counterparts of Λ_n^a, Λ_n^c , respectively. $\mu < 0$, λ_j^a, λ_j^c are eigenvalues of operators $-\Delta \mathcal{L}_2(\phi^c)$, $\mathcal{L}_2(\phi^a)$, and $\mathcal{L}_2(\phi^c)$, respectively; i.e., there exist $\tilde{\psi}$ and $\psi_j^\nu, \nu = a, c$, such that $-\Delta \mathcal{L}_2(\phi^c) \tilde{\psi} = \mu \tilde{\psi}$ and

$$(4.6) \quad \mathcal{L}_2(\phi^\nu) \psi_j^\nu = \lambda_j^\nu \psi_j^\nu, \quad j = 1, 2, \dots, \quad \nu = a, c;$$

the eigenvalues satisfy

$$(4.7) \quad 0 = \lambda_1^a < \lambda_2^a \leq \lambda_3^a \leq \dots \leq \lambda_n^a \leq \dots$$

at metastable state a and

$$(4.8) \quad \lambda_1^c < 0 = \lambda_2^c = \lambda_3^c < \lambda_4^c \leq \dots \leq \lambda_n^c \leq \dots$$

at saddle point c .

4.2. Convergence of the determinant ratio under numerical discretization. Here we study the convergence of (4.4) as $n \rightarrow +\infty$ and thus prove (4.5) rigorously. To do so, we need only prove that the product ratio of nonzero eigenvalues in (4.4) converges to its infinite-dimensional counterpart in (4.5). First of all, it is well known that for fixed index $j > 0$, we have

$$(4.9) \quad \lim_{n \rightarrow +\infty} \lambda_{j,n}^\nu = \lambda_j^\nu, \quad \nu = a, c.$$

Based on this result and estimates of the eigenvalues, we can obtain the following theorem.

THEOREM 4.1. *Let λ_j^a, λ_j^c denote the eigenvalues of $\mathcal{L}_2(\phi^a), \mathcal{L}_2(\phi^c)$ with (4.6), (4.7), (4.8). H^a, H^c are the matrices of the discretization of operators $\mathcal{L}_2(\phi^a), \mathcal{L}_2(\phi^c)$*

in $\mathcal{S}_{r,\mathbf{n}}$, with eigenvalues $\lambda_{j,\mathbf{n}}^a$ and $\lambda_{j,\mathbf{n}}^c$, respectively. Define the discretized determinant ratio and its infinite dimensional counterpart by

$$(4.10) \quad R_{k,\mathbf{n}}^m = \prod_{j=k}^m \lambda_{j,\mathbf{n}}^a / \lambda_{j,\mathbf{n}}^c, \quad R_k^m = \prod_{j=k}^m \lambda_j^a / \lambda_j^c;$$

then $\lim_{\mathbf{n} \rightarrow +\infty} R_{4,\mathbf{n}}^n = R_4^\infty$.

The proof can be found in Appendix B.

4.3. Nucleation rate calculation. First of all, we notice that, once we obtain the saddle point \mathbf{x}^c using GAD method (3.4), the unique negative eigenvalue $\lambda_{1,\mathbf{n}}^c$ and the corresponding normalized eigenvector \mathbf{v}_1^c at saddle point \mathbf{x}^c could be computed following [34, 8], or simply by

$$(4.11) \quad \dot{\mathbf{v}} = -\nabla^2 F_r(\mathbf{x}^c) \mathbf{v} + \frac{\mathbf{v}^T \nabla^2 F_r(\mathbf{x}^c) \mathbf{v}}{\mathbf{v}^T \mathbf{v}} \mathbf{v},$$

with a suitable initial value (for example, $\tilde{\mathbf{v}}_1$), and followed by

$$(4.12) \quad \lambda_{1,\mathbf{n}}^c = (\mathbf{v}_1^c)^T \nabla^2 F_r(\mathbf{x}^c) \mathbf{v}_1^c.$$

In order to compute (4.3), we still need to study algorithms for calculating

$$\frac{\tilde{\det} H^a}{|\tilde{\det} H^c|}.$$

To do this, let

$$(4.13) \quad \tilde{H}^a = H^a + H_0^a, \quad \tilde{H}^c = H^c + H_0^c,$$

where $H_0^a = \mathbf{v}_1^a (\mathbf{v}_1^a)^T$, $H_0^c = \mathbf{v}_2^c (\mathbf{v}_2^c)^T + \mathbf{v}_3^c (\mathbf{v}_3^c)^T - 2\lambda_{1,\mathbf{n}}^c \mathbf{v}_1^c (\mathbf{v}_1^c)^T$. Then \tilde{H}^a, \tilde{H}^c become positive-definite symmetric matrices, and

$$(4.14) \quad \det \tilde{H}^a = \tilde{\det} H^a, \quad \det \tilde{H}^c = |\tilde{\det} H^c|.$$

Thus we need only compute

$$(4.15) \quad \frac{\det \tilde{H}^a}{\det \tilde{H}^c},$$

which is the determinant ratio of two positive-definite symmetric matrices. In the following, we will discuss two possible methods for computing (4.15):

1. Introducing the ensemble average

$$(4.16) \quad Q(\alpha) = \left\langle \frac{1}{2} \mathbf{q}^T (\tilde{H}^a - \tilde{H}^c) \mathbf{q} \right\rangle_\alpha,$$

where $\langle \cdot \rangle_\alpha$ is the expectation under probability distribution

$$(4.17) \quad \pi_\alpha(\mathbf{q}) = \frac{1}{Z_\alpha} \exp \left[-\frac{1}{2} \mathbf{q}^T (\alpha \tilde{H}^c + (1-\alpha) \tilde{H}^a) \mathbf{q} \right],$$

and Z_α is the normalization constant. Then we have [34, 18]

$$(4.18) \quad \frac{\det \tilde{H}^a}{\det \tilde{H}^c} = \exp \left\{ 2 \int_0^1 Q(\alpha) d\alpha \right\}.$$

From (2.9), the Hessian matrices can be written as

$$(4.19) \quad \begin{aligned} H^a &= -\Gamma + J_n^a, \\ H^c &= -\Gamma + J_n^c, \end{aligned}$$

where $\Gamma = -\text{diag}\{\xi^2(1 - \rho_1)^2 + 1, \xi^2(1 - \rho_2)^2 + 1, \dots, \xi^2(1 - \rho_n)^2 + 1\}$ is a negative-definite diagonal matrix. $\forall \mathbf{v} \in \mathbb{R}^n$, the components of $J_n^a \mathbf{v}, J_n^c \mathbf{v}$ are

$$(4.20) \quad \begin{aligned} (J_n^a \mathbf{v})_k &= \left\langle \left[-1 + \tau - \gamma \phi_n^a + \frac{1}{2}(\phi_n^a)^2 \right] \left(\sum_{l=1}^n v_l \omega_l \right), \omega_k \right\rangle, \\ (J_n^c \mathbf{v})_k &= \left\langle \left[-1 + \tau - \gamma \phi_n^c + \frac{1}{2}(\phi_n^c)^2 \right] \left(\sum_{l=1}^n v_l \omega_l \right), \omega_k \right\rangle \end{aligned}$$

for $k = 1, 2, \dots, n$, $\phi_n^\nu = \mathcal{P}_{r,n} \phi^\nu$, and $\|J_n^\nu\|_2$ is uniformly bounded, $\nu = a, c$. Thus with (4.13) we obtain

$$(4.21) \quad \alpha \tilde{H}^c + (1 - \alpha) \tilde{H}^a = -\Gamma + \alpha(J_n^c + H_0^c) + (1 - \alpha)(J_n^a + H_0^a),$$

which can be viewed as a perturbation of the matrix $-\Gamma$, and

$$(4.22) \quad \pi_\alpha(\mathbf{x}) \propto \exp[\mathbf{x}^T \Gamma \mathbf{x} / 2 - \Psi(\mathbf{x})],$$

where

$$(4.23) \quad \Psi(\mathbf{x}) = \frac{1}{2} \mathbf{x}^T \left[\alpha(J_n^c + H_0^c) + (1 - \alpha)(J_n^a + H_0^a) \right] \mathbf{x}.$$

$Q(\alpha)$ can be calculated using the Metropolis–Hastings method following [2]. Supposing the current state is \mathbf{x} , the following Langevin proposal could be used to generate the possible new state \mathbf{y} [2]:

$$(4.24) \quad \mathbf{y} - \mathbf{x} = \left\{ -(1 - \theta)\mathbf{x} - \theta \mathbf{y} - \mathcal{C} \nabla \Psi(\mathbf{x}) \right\} \Delta t + \sqrt{2\Delta t} \boldsymbol{\eta},$$

where $\boldsymbol{\eta} \sim \mathcal{N}(0, \mathcal{C})$, $\mathcal{C} = (-\Gamma)^{-1}$. In the above, Δt is the time step size. Implicit schemes could be obtained with nonzero parameter θ , and $\theta = \frac{1}{2}$ is recommended in [2]. Notice, within Fourier space, that differential terms in (2.9) lead to Γ , which is of diagonal matrix form, and therefore new state \mathbf{y} in implicit scheme (4.24) can be easily solved.

2. Based on the power-series expansion method [1], the following formula is proved in [35].

THEOREM 4.2. *For positive-definite matrix $C \in \mathbb{R}^{N \times N}$, the k -term power-series approximation of $\log \det C$ is*

$$(4.25) \quad \log \det C \approx N \log w - N \mathbb{E} \left(\sum_{j=1}^k \frac{\mathbf{s}^T B^j \mathbf{s}}{j \mathbf{s}^T \mathbf{s}} \right),$$

where $w = \|C\|_\infty$, $B = I - C/w$, and $\mathbf{s} \sim \mathcal{N}_N(0, I)$.

With this formula, the determinant ratio (4.15) could be calculated by

$$(4.26) \quad \frac{\det \tilde{H}^a}{\det \tilde{H}^c} = \frac{\det(C^{\frac{1}{2}} \tilde{H}^a C^{\frac{1}{2}})}{\det(C^{\frac{1}{2}} \tilde{H}^c C^{\frac{1}{2}})} = \exp \left(\log \det(C^{\frac{1}{2}} \tilde{H}^a C^{\frac{1}{2}}) - \log \det(C^{\frac{1}{2}} \tilde{H}^c C^{\frac{1}{2}}) \right).$$

Following [35], the variance of the j th term in (4.25) is

$$\text{Var}\left(\frac{N\mathbf{s}^T B^j \mathbf{s}^T}{j\mathbf{s}^T \mathbf{s}}\right) = \frac{2Nj^{-2}}{N+2} \sum_{l=1}^N \left(\lambda_l^j(B) - \frac{\text{tr}(B^j)}{N}\right)^2 \propto j^{-2},$$

where $\lambda_l(B)$ are eigenvalues of B and $0 \leq \lambda_l(B) < 1$. Suppose n_j random vectors \mathbf{s} are generated to calculate the j th term and all random vectors \mathbf{s} are independent; then the total variance of the estimated log det is of order $\sum_{j=1}^k j^{-2} n_j^{-1}$. For fixed total computational effort, i.e., $\sum_{j=1}^k n_j$ is fixed, using the Cauchy–Schwarz inequality, the variance is minimized when $n_j \propto j^{-1}$. In practice, the same random vector \mathbf{s} will be used in calculating multiple terms, and thus it is not independent. However, we will still use $n_j \propto j^{-1}$ since terms become smaller and less important as j increases.

5. Comparison with the projected Allen–Cahn dynamics. While we are mainly interested in the nucleation of stochastic Cahn–Hilliard dynamics (1.4), some authors [21, 11] studied the evolution of conservative order parameters using projected Allen–Cahn dynamics

$$(5.1) \quad \frac{\partial \phi}{\partial t} = \mathcal{P}\left(-\frac{\delta \mathcal{F}}{\delta \phi} + \sqrt{2\epsilon} \eta\right),$$

where η is the space-time Gaussian white noise satisfying $E(\eta(\mathbf{x}, t)\eta(\mathbf{y}, s)) = \delta(\mathbf{x} - \mathbf{y})\delta(t - s)$, and \mathcal{P} is the orthogonal projection operator onto the mass conserved space $L_{per,0}^2(\Omega)$. In this section, we briefly discuss the differences between these two dynamics.

In the framework of the Galerkin method, the projection operator $\mathcal{P} : L_{per}^2(\Omega) \rightarrow L_{per,0}^2(\Omega)$ is defined by

$$(5.2) \quad \mathcal{P}\phi = \sum_{j \in \mathcal{I}} \langle \phi, e_j \rangle e_j \quad \forall \phi \in L_{per}^2(\Omega).$$

Similarly to (2.11) in section 2, (5.1) is discretized and we obtain the stochastic differential equations of the Fourier coefficients as

$$(5.3) \quad d\phi_j(t) = -\left[\xi^2(1 - \rho_j)^2 \phi_j(t) + Q_j(t)\right] dt + \sqrt{2\epsilon} dW_j(t), \quad j \in \mathcal{I}_n,$$

where $Q_j(t)$ and $W_j(t)$ follow (2.12) and (2.7), respectively, or

$$(5.4) \quad d\mathbf{x} = -\nabla F_r dt + \sqrt{2\epsilon} dW,$$

which is a standard gradient system perturbed by white noise. Following the same lines as in sections 2, 3, and 4, we summarize the results for dynamics (5.1) while focusing on comparing the differences with stochastic Cahn–Hilliard dynamics (1.4):

1. The metastable states of dynamical system

$$(5.5) \quad \frac{\partial \phi}{\partial t} = -\mathcal{P} \frac{\delta \mathcal{F}}{\delta \phi}$$

could be located using the semi-implicit spectral method [4]:

$$(5.6) \quad \left[1 + \xi^2 \Delta t (1 - \rho_j)^2\right] \phi_j^{k+1} = \phi_j^k - \Delta t Q_j^k, \quad j \in \mathcal{I}_n, \quad k = 0, 1, 2, \dots,$$

where Δt is the time step size, and Q_j^k follows (2.12). Comparing (5.5) with (1.3), since $\mathcal{P} \frac{\delta \mathcal{F}}{\delta \phi} = 0$ is equivalent to $\Delta \frac{\delta \mathcal{F}}{\delta \phi} = 0$ in $L^2_{per,0}(\Omega)$, we know that they share the same equilibrium states of the same type, which are the metastable states and saddle points of the energy functional \mathcal{F} in $L^2_{per,0}(\Omega)$. Especially, the lamellar phase a , cylinder phase b , and saddle point c can be obtained using both (3.1) and (5.6).

2. With (5.4), the MEP $u^*(\cdot, t) \in \mathbb{R}^n$ connecting two metastable states a (lamellar phase) and b (cylinder phase) of system (5.1) is described by the concatenation of two parts

$$(5.7) \quad \lim_{t \rightarrow -\infty} u^*(t) = a, \quad \lim_{t \rightarrow +\infty} u^*(t) = c, \quad \frac{du^*}{dt} = \nabla F_r$$

and

$$(5.8) \quad \lim_{t \rightarrow -\infty} u^*(t) = c, \quad \lim_{t \rightarrow +\infty} u^*(t) = b, \quad \frac{du^*}{dt} = -\nabla F_r,$$

where $c \in \partial\Omega(a) \cap \partial\Omega(b)$ is the saddle point. Comparing with (3.2) and (3.3), we conclude that while the endpoints a, b, c of the MEPs are the same in both dynamics, the MEPs are essentially different. Especially, at the saddle point c , while the tangent direction $\tilde{\psi}$ of the MEP for dynamics (1.4) satisfies $-\Delta \mathcal{L}_2(\phi^c) \tilde{\psi} = \mu \tilde{\psi}$, $\mu < 0$, the tangent direction of the MEP for dynamics (5.1) coincides with the negative eigenfunction ψ_1^c of operator $\mathcal{L}_2(\phi^c)$.

3. Following [30, 34], the nucleation rate of system (5.4) can be obtained as

$$(5.9) \quad k_n = \frac{1}{2\pi} (2\pi\epsilon)^{-\frac{1}{2}} \left(|\lambda_{1,n}^c| \lambda_{2,n}^a \lambda_{3,n}^a \right)^{\frac{1}{2}} \left(\prod_{j=4}^n \lambda_{j,n}^a / \lambda_{j,n}^c \right)^{\frac{1}{2}} \frac{L_x \Lambda_n^c}{\Lambda_n^a} e^{-\frac{\Delta F_r}{\epsilon}}.$$

When $n \rightarrow +\infty$, the nucleation rate formula for projected Allen–Cahn equation (5.1) with periodic BC is obtained as

$$(5.10) \quad k = \frac{1}{2\pi} (2\pi\epsilon)^{-\frac{1}{2}} \left(|\lambda_1^c| \lambda_2^a \lambda_3^a \right)^{\frac{1}{2}} \left(\prod_{j=4}^{+\infty} \lambda_j^a / \lambda_j^c \right)^{\frac{1}{2}} \frac{L_x \Lambda^c}{\Lambda^a} e^{-\frac{\Delta F_r}{\epsilon}},$$

where all the variables have the same meaning as in section 4.1. Comparing to the nucleation rate formulas (4.4) and (4.5) for stochastic Cahn–Hilliard equation (1.4), we can see the tiny difference in the prefactor.

6. Numerical results. We choose parameters $\xi^2 = 1.0$, $\tau = -0.15$, $\gamma = 0.25$ in Landau–Brazovskii energy functional (1.1). With these parameters, the lamellar phase and the cylinder phase are two equilibrium phases, while the cylinder phase has lower energy and therefore is more stable. In the following, we will focus on the nucleation event from the lamellar phase to the cylinder phase.

6.1. Validation on small domain. To check the correctness of our numerical results, we first study the nucleation event on a small domain $\Omega = [0, \frac{16\pi}{\sqrt{3}}] \times [0, 8\pi]$ with $n_1 = n_2 = 60$. The MEP and the saddle point could be obtained using the string method and the GAD method. The string is discretized into 21 nodes and is iterated with $\Delta t = 0.1$ for 10000 steps. After that, the first (lamellar phase) and last node (cylinder phase) on the string are converged with residual smaller than 10^{-13} . The

energy densities of these two nodes are -2.267×10^{-2} and -2.375×10^{-2} , respectively. The 12th node on the string has the maximum energy, and the residual is 9.96×10^{-6} . Using this node as the initial value of the saddle point and approximating the tangent direction of the MEP at the saddle point by the finite difference method, we could compute the saddle point and tangent direction of the MEP at saddle point with GAD method (3.4) precisely. The time step size is $\Delta t = 0.1$, and the semi-implicit spectral method similar to (3.1) is used. At the k th step, denote the L^∞ norm of the right-hand side of (3.4) by r^k , and let

$$(6.1) \quad r_1^k = \frac{\mathbf{v}^T \nabla F_r(\mathbf{x})}{\mathbf{v}^T G^{-1} \mathbf{v}}, \quad r_2^k = \frac{\mathbf{v}^T \nabla^2 F_r(\mathbf{x}) \mathbf{v}}{\mathbf{v}^T G^{-1} \mathbf{v}}.$$

When $k = 0$, we have $r^0 = 1.50 \times 10^{-3}$, $r_1^0 = 1.60 \times 10^{-5}$, $r_2^0 = -0.02107$. After 9900 iterations, we obtain $r^{9900} = 1.93 \times 10^{-14}$, $r_1^{9900} = 1.24 \times 10^{-14}$, $r_2^{9900} = -0.021177$. From r^{9900} and r_1^{9900} we could conclude the convergence of the GAD method, and the saddle point is obtained with $\mu_{1,\mathbf{n}} = -0.021177$. The energy density of the saddle point is -2.238×10^{-2} , and hence the barrier of energy density is 2.9×10^{-4} . From (4.11) and (4.12), we obtain $\lambda_{1,\mathbf{n}}^c = -0.0211718$. The lamellar phase, the cylinder phase, and the saddle point are shown in Figure 6.1, and we can see that the shape of the critical nucleus is affected by the physical boundaries since we choose a small domain.

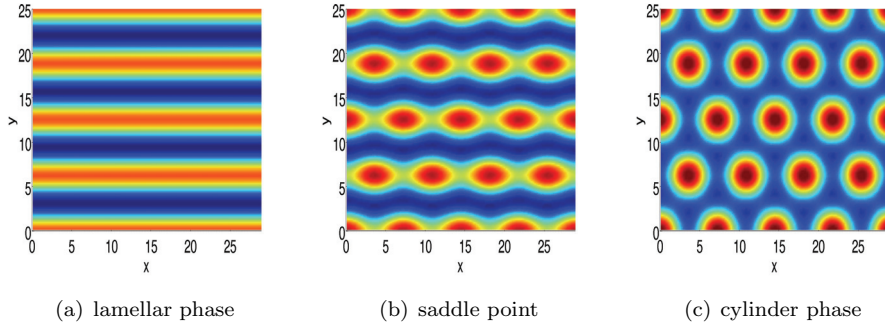


FIG. 6.1. Lamellar phase, cylinder phase, and saddle point computed using semi-implicit spectral scheme (3.1) and the GAD method. $\Omega = [0, \frac{16\pi}{\sqrt{3}}] \times [0, 8\pi]$, $\xi^2 = 1.0$, $\tau = -0.15$, $\gamma = 0.25$. The number of basis functions is $n_1 = n_2 = 60$. The energy densities are -2.267×10^{-2} , -2.238×10^{-2} , and -2.375×10^{-2} , respectively, with the barrier of energy density equal to 2.9×10^{-4} .

For comparison, we also have some results about the string method with the finite difference method in Remark 1. On the same domain Ω , the explicit Euler scheme is used to update (2.19) with time t . We take $N_x = N_y = 32$ and $\Delta t = 0.001$. After 975000 iterations, the residual's norms at two endpoints on the string are of order 10^{-14} , while they are of order 10^{-7} at the maximum energy node. However, this grid is rather coarse. If we take $N_x = N_y = 64$ (this grid is still not fine enough actually; see section 7 for further discussions), the time step size Δt is further limited and we choose $\Delta t = 10^{-5}$ in the experiment. After 1565000 iterations, the residual's norms at two endpoints are of order 10^{-6} , while they are of order 10^{-3} at the maximum energy node. Therefore the convergence becomes very slow. The fact that the time step size with the semi-implicit spectral method could be several orders of magnitude larger than that with the explicit finite difference method is demonstrated in [4].

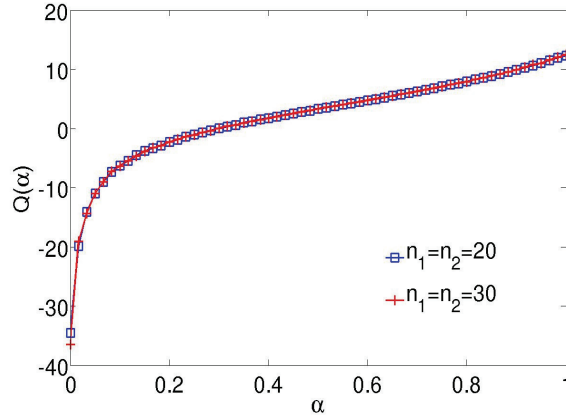


FIG. 6.2. $Q(\alpha)$ as a function of α . $\Omega = [0, \frac{16\pi}{\sqrt{3}}] \times [0, 8\pi]$, $\xi^2 = 1.0$, $\tau = -0.15$, $\gamma = 0.25$. The numbers of basis functions are $n_1 = n_2 = 20$ and $n_1 = n_2 = 30$, respectively. $\alpha \in [0, 1]$ is discretized to 60 nodes. 600000 steps are used when calculating $Q(\alpha)$ for each α .

TABLE 6.1

The logarithm of the determinant ratio computed by solving all the eigenvalues of the Hessian matrices using Lapack software (I), the MCMC method (II), and the power-series expansion method (III). The numbers of basis functions are $n_1 = n_2 = 20$ and $n_1 = n_2 = 30$, respectively. The results for methods II and III are the mean values of five runs.

	I	II	III
$n_1 = n_2 = 20$	4.32	4.34	4.33
$n_1 = n_2 = 30$	4.34	4.36	4.35

To check the results, we choose $n_1 = n_2 = 20$ and $n_1 = n_2 = 30$, respectively. In these two cases, with the GAD method and (4.11), (4.12), we also have $\mu_{1,\mathbf{n}} = -0.021177$ and $\lambda_{1,\mathbf{n}}^c = -0.0211718$. These results are examined by computing the smallest eigenvalue of the Hessian matrix using Lapack software, and the same results are obtained. Thus we conclude that the method is correct and that the results are not sensitive for different numbers of basis functions \mathbf{n} .

For the determinant ratio, we compute its logarithm by directly solving the eigenvalues of the Hessian matrix using Lapack software, the MCMC method, and the power-series expansion method introduced above. When using the MCMC method, the interval $[0, 1]$ for α is discretized into 60 points and 60 processors are utilized. 600000 steps have been used while calculating $Q(\alpha)$ for each α , and the results are shown in Figure 6.2. When using the power-series expansion method, the series are expanded to 1000 terms and codes are parallelized to reduce the total computational time. As mentioned above, for the j th term, the number of random vectors for computing the expectation is

$$(6.2) \quad \min \left\{ 500000, \max \left\{ \frac{500000 \times 5}{j}, 10 \right\} \right\};$$

that is, the number is decreasing as j increases while maintaining in $[10, 500000]$. Table 6.1 compares the numerical results of the determinant ratio with these three methods.

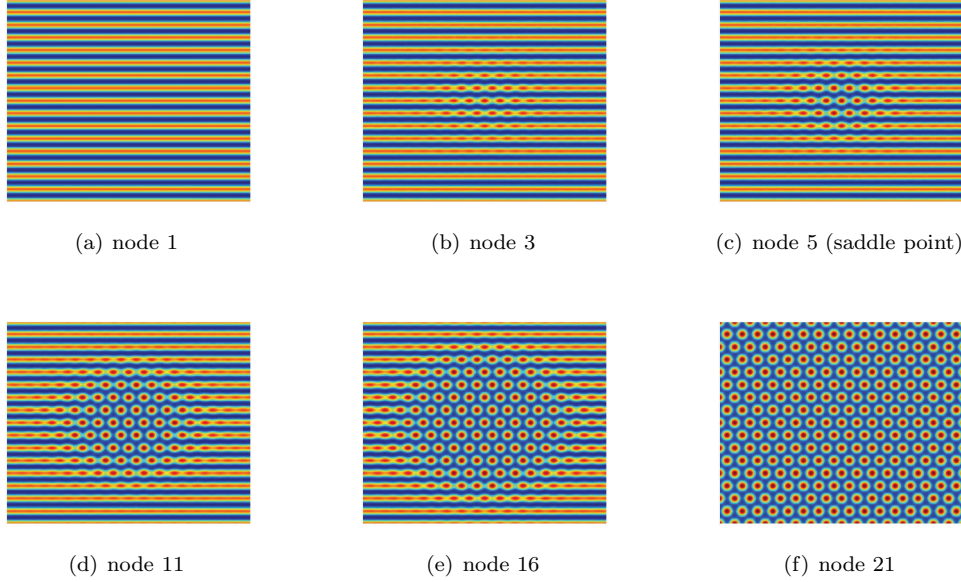


FIG. 6.3. $\Omega = [0, \frac{64\pi}{\sqrt{3}}] \times [0, 32\pi]$. $\xi^2 = 1.0$, $\tau = -0.15$, $\gamma = 0.25$ nodes on the MEP for the nucleation from the lamellar phase to the cylinder phase. 21 nodes are used along the MEP. Semi-implicit spectral method (3.1) is used, with time step $\Delta t = 0.1$. 40000 iterations are performed. The node along the MEP with the maximum energy is shown in (c). We could see that, during nucleation from the lamellar phase to the cylinder phase, a small nucleus first pops out from the middle of the domain and then grows up until the whole domain transitions to the cylinder phase.

6.2. Nucleation event study from lamellar phase to cylinder phase. Now we consider a larger domain $\Omega = [0, \frac{64\pi}{\sqrt{3}}] \times [0, 32\pi]$, and the number of basis functions is $n_1 = n_2 = 100$. While using the string method in Fourier space (Algorithm 1), the string is discretized to 21 nodes and the time step size is $\Delta t = 0.1$ with the semi-implicit spectral method. The string is converged after 40000 iterations, and the MEP is shown in Figure 6.3, on which the 5th node has the maximum energy and therefore corresponds to the saddle point (critical nucleus). We could see the transition process from the lamellar phase to the cylinder phase gradually. The energy density along the MEP is shown in Figure 6.5(a), where the energy density barrier (i.e., $\Delta\mathcal{F}/V$) equals 5.357×10^{-5} .

After the convergence of the MEP, using the node which has the maximum energy density on the MEP (Figure 6.3(c)) as the initial value of the saddle point and approximating the tangent direction of the MEP at the saddle point by the finite difference method, we could compute the saddle point and tangent direction of the MEP at the saddle point with GAD method (3.4) precisely. The time step size is $\Delta t = 0.1$, and the semi-implicit spectral method similar to (3.1) is used. At the k th step, denote r^k, r_1^k, r_2^k as in (6.1). We have $r^0 = 1.50 \times 10^{-3}$, $r_1^0 = 2.93 \times 10^{-5}$, $r_2^0 = -8.43 \times 10^{-3}$ at the beginning of the iteration $k = 0$. After 39900 iterations, $r^{39900} = 4.32 \times 10^{-13}$, $r_1^{39900} = -4.45 \times 10^{-13}$, $r_2^{39900} = -8.01 \times 10^{-3}$. The state's energy density varies slightly (smaller than 2×10^{-7}) during iterations, and the energy density of the converged state is -2.25187×10^{-2} (the corresponding energy density barrier $\Delta F_r = 5.34 \times 10^{-5}$). By observing r^{39900} and r_1^{39900} , it is obvious

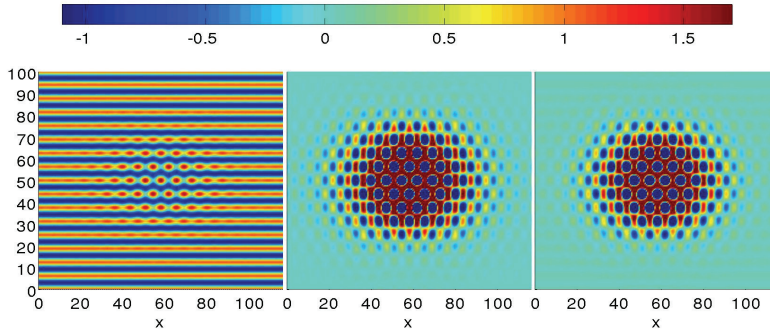


FIG. 6.4. $\Omega = [0, \frac{64\pi}{\sqrt{3}}] \times [0, 32\pi]$. $\xi^2 = 1.0$, $\tau = -0.15$, $\gamma = 0.25$. *Left panel: the precise saddle point. Middle panel: the tangent direction of the MEP at the saddle point for stochastic Cahn–Hilliard dynamics (1.4). Right panel: the tangent direction of the MEP at the saddle point for stochastic projected Allen–Cahn dynamics (5.1). They are computed using GAD method (3.4) and (4.11). Comparing these two tangent directions, we can see that the wave of the tangent direction in the middle panel decays slower, which indicates a wider interface in the tangent direction of the MEP for stochastic Cahn–Hilliard dynamics (1.4).*

that the GAD method with the semi-implicit spectral method performs very well, and the right-hand side of the generalized gradient system (2.17) is zero for the converged state. r_2^{39900} indicates that $\mu_{1,n}$, the unique negative eigenvalue of the matrix $G\nabla^2 F_r(\mathbf{x}^c)$, is -8.01×10^{-3} . The precise saddle point \mathbf{x}^c , the MEP’s tangent direction $\tilde{\mathbf{v}}_1$ at \mathbf{x}^c , and the eigenvector \mathbf{v}_1^c of $\nabla^2 F_r(\mathbf{x}^c)$ are shown in Figure 6.4. From (4.11), (4.12), we obtain $\lambda_{1,n}^c = -0.0131$.

For the determinant ratio, in this case it is not feasible to use Lapack to compute all the eigenvalues since the size of the matrix is very large, and the MCMC method does not give a satisfactory result due to difficulties in high-dimensional sampling. On the contrary, with the power-series method, we take 1000 terms in the power-series expansion. A nonuniform number of random vectors is used for different terms in order to reduce computations. Specifically, for the j th term, the number of random vectors generated for computing the expectation is (comparing to (6.2))

$$(6.3) \quad \min \left\{ 1000000, \frac{1000000 \times 4}{j} \right\}.$$

The mean value of the logarithm of the determinant ratio for five runs is 17.17 with variance equals 0.0185. All the quantities in (4.3) are summarized in Table 6.2 and are used to compute the nucleation rate for different noise intensity ϵ , as shown in Figure 6.5(b). It is noteworthy that the prefactor in (4.3) has a significant contribution in the final nucleation rate.

TABLE 6.2

The quantities in the nucleation rate formula (4.3). LDR refers to the logarithm of the determinant ratio. $\Omega = [0, \frac{64\pi}{\sqrt{3}}] \times [0, 32\pi]$. $\xi^2 = 1.0$, $\tau = -0.15$, $\gamma = 0.25$. $n_1 = n_2 = 100$.

$\lambda_{1,n}^c$	$\mu_{1,n}$	Λ_n^a	Λ_n^c	LDR	ΔF_r
-0.0131	-8.01×10^{-3}	0.78	0.072	17.17	5.34×10^{-5}

For comparison, we also compute the results for the stochastic projected Allen–Cahn dynamics (5.1). Although the MEP of dynamics (5.1) is different from that of

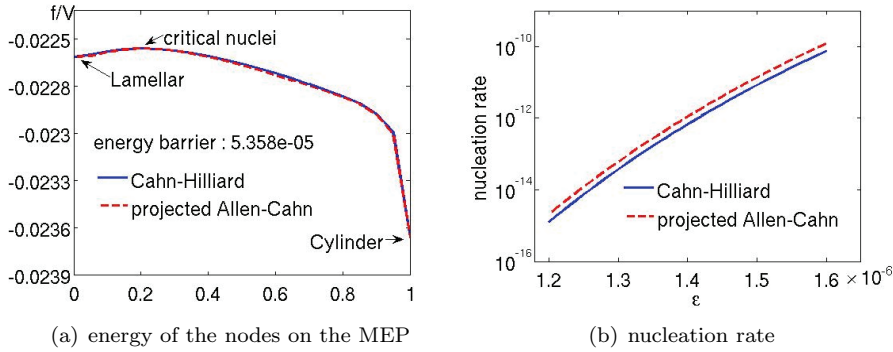


FIG. 6.5. $\Omega = [0, \frac{64\pi}{\sqrt{3}}] \times [0, 32\pi]$. $\xi^2 = 1.0$, $\tau = -0.15$, $\gamma = 0.25$. Energy profile along the MEPs and the nucleation rate with both stochastic Cahn–Hilliard dynamics (1.4) and projected Allen–Cahn dynamics (5.1). (a) The 5th node is the maximum energy node on the MEP, and the barrier of the energy density is 5.358×10^{-5} . The x-axis is the arclength parameter, and the y-axis is the density of the free energy functional \mathcal{F}/V . Although the energy curves of these two dynamics are quite similar, the MEPs are different. (b) The nucleation rate from the lamellar phase to the cylinder phase with different noise intensity.

the stochastic Cahn–Hilliard dynamics (1.4), the difference is small and indistinguishable (Figure 6.3). The energy profiles along the MEPs for both dynamics are shown in Figure 6.5(a). We emphasize that it is not convincing to tell whether the MEPs for these two dynamics are different from this figure, because only several (21) nodes are used to discretize the MEP in the high-dimensional path space, and the energy profile is just a 1D projection of the MEP. In Figure 6.4, we can see that the tangent directions of the MEP at the saddle point are different for these two dynamics. The wave of the tangent direction for the stochastic Cahn–Hilliard dynamics (1.4) (the middle panel in Figure 6.4) decays slower than that for the projected Allen–Cahn dynamics (5.1) (the right panel in Figure 6.4), which indicates a wider interface in the tangent direction of the MEP for the stochastic Cahn–Hilliard dynamics. Due to the different values of $\lambda_{1,n}^c$ and $\mu_{1,n}$ (see Table 6.2), the nucleation rates for both dynamics, given by (4.4) and (5.9), are also different and are shown in Figure 6.5(b).

7. Discussions. Following the previous 1D work [34], we study the nucleation rate calculation for diblock copolymers. The dynamics of diblock copolymers is described by the 2D stochastic Cahn–Hilliard dynamics with a Landau–Brazovskii energy functional. To achieve this, we need to study the MEP of the nucleation event and the saddle point on it. The string method and the GAD method are designed in Fourier space and are combined with the semi-implicit method. Both the MEP and saddle point can be obtained efficiently.

Although the existence and regularity of the solution for dynamics (1.4) are beyond the scope of the present work, we want to make a brief comment here. In [25], the authors have proved the regularity of the solution under condition

$$(7.1) \quad \text{Tr}(A^{-1+\delta}Q) < \infty \text{ for some } \delta > 0,$$

where A is the Laplacian operator with certain BC, and Q is the covariance matrix of the Wiener process in the noise term. From this conclusion, the authors in [25] conclude that while the linear part regularizes the solution, the noise term makes it worse. And the regularity of the solution depends on the competition of these two

terms. In our case, the higher order linear terms in (1.4) have stronger regularization effects, and thus we believe its solution has better regularity.

In our previous work [34], we used the finite difference method (FDM) to study 1D Cahn–Hilliard dynamics with a simpler energy functional. In this work, however, although we could still discretize the problem with FDM as illustrated in Remark 1, there are several drawbacks. First, due to the high order differential terms in the dynamics equation, very fine grids are needed in order to obtain accurate approximation, which then leads to a very small time step size when solving the equation and a very large Hessian matrix when computing the determinant. Second, the determinant ratio of two differential operators is needed and is approximated by the ratio of two Hessian matrices numerically. With FDM, the large eigenvalues of the Hessian matrices will be very different from their counterparts of the original differential operators, simply because the corresponding eigenvectors have high frequency and are not well approximated by FDM. On the other hand, these eigenvalues could still be close to their true values relatively (see Appendix B) with spectral discretization since the subspace is spanned by the eigenfunctions of the Laplacian operator.

For the nucleation rate, since we focus on the numerical algorithms, the convergence of (4.3), (4.4) is assumed and we give the nucleation rate formula (4.5) without proof. Numerically, we always need to discretize the original problem (1.4) with a finite number of basis functions and compute the nucleation rate using (4.3), (4.4). What is more, for a given number of basis functions, only small eigenvalues of the original problems can be approximated precisely and larger ones cannot. Even with this, the convergence of the determinant ratio could be obtained assuming that the finite trace of the linear part’s inverse operator in the stochastic PDE, which is also related to the regularity of the stochastic PDEs’ solutions, and that every single eigenvalue converges to its infinite-dimensional counterpart as more modes are involved. These assumptions are quite loose and generally hold in a wide range of stochastic PDE models [26]. Thus the proof should also apply to those models to obtain the convergence result for the determinant ratio.

Besides the MCMC method used in our previous work [34], we try the power-series expansion method [35] to compute the determinant ratio. With this method, the line integration in (4.18) can be avoided and the number of random vectors to calculate expectation is chosen nonuniformly for different expanded terms. However, on a large physical domain with a huge number of basis functions, due to the high dimension of the matrix size, both methods, even utilizing parallel computing, are time consuming in order to obtain an accurate result of the logarithm of the determinant.

We also compare the dynamics of the stochastic Cahn–Hilliard equation (1.4) with the projected Allen–Cahn equation (5.1), which can also describe the dynamics of conservative order parameters. We conclude that both the MEP and the nucleation rate are different for these two dynamics.

For BCs, besides periodic BC considered here, Neumann BC is also frequently proposed in the study of Cahn–Hilliard equations. Generally, based on our understanding, periodic BC is mathematically simple and is often used in material structure as well as molecule dynamics simulations, especially when periodicity exists (as in the case of diblock copolymer) or when the size of the whole system is far beyond the computational ability, and thus only part of it is simulated. On the other hand, Neumann BC is used when we want to simulate the whole system and assume that there is no flux coming from the boundaries. In our work, the size of the domain is chosen to be larger than the diameter of the critical nucleus, thus assuming BC has a tiny impact on its shape. Similar to periodic BC, Neumann BC could also be studied with mi-

nor modifications. First, we could consider the subspace spanned by bases satisfying Neumann BC. These bases consist of functions of the form $C \cos(k_1 \frac{2\pi x}{L_1}) \cos(k_2 \frac{2\pi y}{L_2})$, where $k_1, k_2 \in \mathbb{Z}$, C is the normalization constant. Second, numerically, the FFT method may need to be modified in order to find the Fourier coefficients from the real space and vice versa. Third, different from the periodic case, there is no translation invariance anymore with Neumann BC, and thus the Hessian matrices at metastable states and saddle point are nondegenerate. The prefactor in the nucleation rate formula is also slightly different (see [34] for details in 1D Cahn–Hilliard dynamics).

The ideas and methods discussed in this paper are general for the nucleation rate calculation (and the nucleation event) in zero temperature limit. The issues of nucleation at finite temperature and on large domains are untouched, and we refer the reader to [34, 16, 30] for discussions. In future work, we may consider applying these methods to study the nucleation event between other ordered phases (from the cylinder phase to the sphere phase, etc.) in diblock copolymers, or even the nucleation events for other stochastic PDE models.

8. Conclusions. In this paper, we study the nucleation rate calculation for diblock copolymers by considering the 2D stochastic Cahn–Hilliard dynamics with a Landau–Brazovskii energy functional. The nucleation rate for phase transition from the lamellar phase to the cylinder phase of diblock copolymers is investigated. Under the framework of the spectral method, we design the string method and the GAD method in Fourier space. These two methods, when combined with the semi-implicit spectral method, are very efficient for computing the MEP and the saddle point. The nucleation rate formula is also given, and related numerical algorithms are discussed with careful implementations.

Appendix A. Galerkin discretization for stochastic Cahn–Hilliard equation. Here we consider the Galerkin discretization for the 2D stochastic Cahn–Hilliard equation (1.4) on domain $\Omega = [0, L_x] \times [0, L_y]$ with periodic BC. Let $V = |\Omega|$. For indices’ operations in (2.2), $\forall \mathbf{j} = (j_1, j_2)$, $\mathbf{k} = (k_1, k_2) \in \mathcal{I}$, we define

$$\begin{aligned} \mathbf{j} \pm \mathbf{k} &= (j_1 \pm k_1, j_2 \pm k_2), \quad -\mathbf{j} = (-j_1, -j_2), \quad |\mathbf{j}| = (|j_1|, |j_2|), \\ \mathbf{j} \leq \mathbf{k} &\iff j_1 \leq k_1, j_2 \leq k_2. \end{aligned}$$

With the basis functions (2.3), (2.4) defined in section 2, we define the spaces $\mathcal{S} = \text{span}\{e_{\mathbf{j}}, \mathbf{j} \in \mathcal{I}\}$, $\mathcal{S}_r = \text{span}\{e_{j,1}, e_{j,2}, \mathbf{j} \in \mathcal{I}_r\}$, which are two (complex and real, respectively) Hilbert spaces with inner products

$$(A.1) \quad \langle f, g \rangle = \frac{1}{|\Omega|} \int_{\Omega} f \bar{g} \, d\mathbf{r} \quad \forall f, g \in \mathcal{S},$$

$$(A.2) \quad \langle f, g \rangle_r = \frac{1}{|\Omega|} \int_{\Omega} f g \, d\mathbf{r} \quad \forall f, g \in \mathcal{S}_r.$$

In fact, we have

$$\mathcal{S}_r = \left\{ \phi \in L^2(\Omega) \mid \frac{1}{V} \int_{\Omega} \phi(\mathbf{r}) \, d\mathbf{r} = 0 \right\} = \left\{ \phi \text{ is real} \mid \phi \in \mathcal{S} \right\}.$$

$\{e_{\mathbf{j}}\}_{\mathbf{j} \in \mathcal{I}}$, $\{e_{j,1}, e_{j,2}\}_{\mathbf{j} \in \mathcal{I}_r}$ form the orthonormal bases of \mathcal{S} and \mathcal{S}_r , respectively. In the following, we will omit the subscripts and use $\langle \cdot, \cdot \rangle$ to denote the inner product on both \mathcal{S} and \mathcal{S}_r .

The Q-Wiener process $W(t)$ in (1.4) is given by (2.6). The covariance operator $Q = -\Delta$ of $W(t)$ is defined on \mathcal{S}_r by

$$(A.3) \quad Qe_{j,\nu} = \rho_j e_{j,\nu}, \quad \nu = 1, 2, \quad \forall \mathbf{j} \in \mathcal{I}_r,$$

where $\rho_j = (2\pi k/L_x)^2 + (2\pi l/L_y)^2$, $\mathbf{j} = (k, l) \in \mathcal{I}_r$.

For Galerkin discretization, let $n_1, n_2 \in \mathbb{N}^+$, $\mathbf{n} = (n_1, n_2)$, consider index subsets

$$(A.4) \quad \mathcal{I}_{\mathbf{n}} = \left\{ (k, l) \in \mathcal{I} \mid |(k, l)| \leq \mathbf{n} \right\}, \quad \mathcal{I}_{r,\mathbf{n}} = \left\{ (k, l) \in \mathcal{I}_r \mid |(k, l)| \leq \mathbf{n} \right\},$$

and consider subspaces $\mathcal{S}_{\mathbf{n}} = \text{span}\{e_{\mathbf{j}}, \mathbf{j} \in \mathcal{I}_{\mathbf{n}}\}$, $\mathcal{S}_{r,\mathbf{n}} = \text{span}\{e_{j,1}, e_{j,2}, \mathbf{j} \in \mathcal{I}_{r,\mathbf{n}}\}$.

The projection operators $\mathcal{P}_{\mathbf{n}}, \mathcal{P}_{r,\mathbf{n}}$ on subspaces $\mathcal{S}_{\mathbf{n}}, \mathcal{S}_{r,\mathbf{n}}$ are given by

$$(A.5) \quad \mathcal{P}_{\mathbf{n}}\phi = \sum_{\mathbf{j} \in \mathcal{I}_{\mathbf{n}}} \phi_{\mathbf{j}} e_{\mathbf{j}}, \quad \phi_{\mathbf{j}} = \langle \phi, e_{\mathbf{j}} \rangle \quad \forall \phi \in \mathcal{S},$$

$$(A.6) \quad \mathcal{P}_{r,\mathbf{n}}\phi = \sum_{\mathbf{j} \in \mathcal{I}_{r,\mathbf{n}}} (\phi_{j,1} e_{j,1} + \phi_{j,2} e_{j,2}), \quad \phi_{j,\nu} = \langle \phi, e_{j,\nu} \rangle, \quad \nu = 1, 2, \quad \forall \phi \in \mathcal{S}_r.$$

When $\phi \in \mathcal{S}_r$, the coefficients satisfy

$$(A.7) \quad \phi_{j,1} = \frac{1}{\sqrt{2}}(\phi_{\mathbf{j}} + \overline{\phi_{\mathbf{j}}}), \quad \phi_{j,2} = \frac{i}{\sqrt{2}}(\phi_{\mathbf{j}} - \overline{\phi_{\mathbf{j}}}), \quad \mathbf{j} \in \mathcal{I}_{r,\mathbf{n}},$$

and $\phi_{\mathbf{j}} = \overline{\phi_{-\mathbf{j}}}$ $\forall \mathbf{j} \in \mathcal{I}_{\mathbf{n}}$ since ϕ is real.

The Galerkin method for stochastic Cahn–Hilliard equation (1.4) on subspace $\mathcal{S}_{\mathbf{n}}$ is given in (2.10), (2.11), (2.12), while on subspace $\mathcal{S}_{r,\mathbf{n}}$, the Galerkin method for (1.4) is to find $\phi^r(\cdot, t) = \sum_{\mathbf{j} \in \mathcal{I}_{r,\mathbf{n}}} (a_{\mathbf{j}}(t)e_{j,1} + b_{\mathbf{j}}(t)e_{j,2}) \in \mathcal{S}_{r,\mathbf{n}}$, which solves

$$(A.8) \quad \langle d\phi^r(\cdot, t) - \Delta \mathcal{L}_1(\phi^r(\cdot, t))dt, e_{j,l} \rangle = \langle \sqrt{2\epsilon}dW(t), e_{j,l} \rangle = \sqrt{2\epsilon\rho_j}dW_{j,l}, \\ l = 1, 2, \quad \forall \mathbf{j} \in \mathcal{I}_{r,\mathbf{n}}.$$

We order the indices in $\mathcal{I}_{r,\mathbf{n}}$ and denote $\mathcal{I}_{r,\mathbf{n}} = \{\mathbf{j}_1, \mathbf{j}_2, \dots, \mathbf{j}_{n_r}\}$, with $\#\mathcal{I}_{r,\mathbf{n}} = n_r = 2n_1n_2 + n_1 + n_2$ and $n = 2n_r$. Rewrite the coefficients $a_{\mathbf{j}}(t), b_{\mathbf{j}}(t)$, the basis functions $e_{j,1}, e_{j,2}$, and the Brownian motions $W_{j,1}, W_{j,2}$ in vector form as

$$(A.9) \quad \mathbf{x} = (x_1(t), x_2(t), \dots, x_n(t))^T \\ = (a_{j_1}(t), a_{j_2}(t), \dots, a_{j_{n_r}}(t), b_{j_1}(t), b_{j_2}(t), \dots, b_{j_{n_r}}(t))^T,$$

$$(A.10) \quad \boldsymbol{\omega} = (\omega_1, \omega_2, \dots, \omega_n)^T = (e_{j_1,1}, e_{j_2,1}, \dots, e_{j_{n_r},1}, e_{j_1,2}, e_{j_2,2}, \dots, e_{j_{n_r},2})^T,$$

$$(A.11) \quad D = (D_1, D_2, \dots, D_n)^T \\ = (\rho_{j_1}, \rho_{j_2}, \dots, \rho_{j_{n_r}})^T = (\rho_{j_1}, \rho_{j_2}, \dots, \rho_{j_{n_r}}, \rho_{j_1}, \rho_{j_2}, \dots, \rho_{j_{n_r}})^T,$$

$$(A.12) \quad W = (W_1(t), W_2(t), \dots, W_n(t))^T \\ = (W_{j_1,1}(t), W_{j_2,1}(t), \dots, W_{j_{n_r},1}(t), W_{j_1,2}(t), W_{j_2,2}(t), \dots, W_{j_{n_r},2}(t))^T.$$

Then (A.8) is equivalent to

$$(A.13) \quad dx_l = -D_l \langle \mathcal{L}_1(\phi^r), \omega_l \rangle dt + \sqrt{2\epsilon D_l} dW_l, \quad l = 1, 2, \dots, n.$$

Let $F_r(\mathbf{x}) = \mathcal{F}(\phi^r)/V$, $\phi^r = \sum_{l=1}^n x_l \omega_l$; then it is straightforward to check that

$$(A.14) \quad \frac{\partial F_r}{\partial x_l} = \langle \mathcal{L}_1(\phi^r), \omega_l \rangle, \quad l = 1, 2, \dots, n.$$

With the notations $G = \text{diag}\{D_1, D_2, \dots, D_n\}$, $\nabla F_r = (\frac{\partial F_r}{\partial x_1}, \frac{\partial F_r}{\partial x_2}, \dots, \frac{\partial F_r}{\partial x_n})^T$, from (A.13), we obtain a generalized stochastic gradient system in \mathbb{R}^n :

$$(A.15) \quad d\mathbf{x} = -G\nabla F_r dt + \sqrt{2\epsilon}G^{\frac{1}{2}}dW.$$

The Galerkin discretization of the deterministic Cahn–Hilliard equation (1.3) could be obtained in the same way by dropping the stochastic terms, and we have

$$(A.16) \quad \frac{d\phi_j(t)}{dt} = -\rho_j \langle \mathcal{L}_1(\phi^c(\cdot, t)), e_j \rangle = -\rho_j \left\{ \xi^2(1 - \rho_j)^2 \phi_j(t) + Q_j(t) \right\}, \quad j \in \mathcal{I}_n,$$

and

$$(A.17) \quad \frac{d\mathbf{x}}{dt} = -G\nabla F_r.$$

Appendix B. Proof for the convergence of determinant ratio. Here we give the proof for the convergence of the determinant ratio.

THEOREM B.1. *Let λ_j^a, λ_j^c denote the eigenvalues of $\mathcal{L}_2(\phi^a), \mathcal{L}_2(\phi^c)$ with (4.6), (4.7), (4.8). H^a, H^c are the matrices of the discretization of operators $\mathcal{L}_2(\phi^a), \mathcal{L}_2(\phi^c)$ in $\mathcal{S}_{r,n}$, with eigenvalues $\lambda_{j,n}^a$ and $\lambda_{j,n}^c$, respectively. Define the discretized determinant ratio and its infinite dimensional counterpart by*

$$(B.1) \quad R_{k,n}^m = \prod_{j=k}^m \lambda_{j,n}^a / \lambda_{j,n}^c, \quad R_k^m = \prod_{j=k}^m \lambda_j^a / \lambda_j^c;$$

then $\lim_{n \rightarrow +\infty} R_{4,n}^n = R_4^\infty$.

Proof. First of all, we notice the decomposition (4.19) and the uniform boundness of $\|J_n^\nu\|_2$, $\nu = a, c$ (see section 4.3). By the min-max theorem for the eigenvalues of a self-adjoint operator, there exists constant $M > 0$ such that

$$(B.2) \quad \xi^2(1 - \rho_j)^2 - M \leq \lambda_{j,n}^\nu \leq \xi^2(1 - \rho_j)^2 + M, \quad j = 1, 2, \dots, n, \quad \nu = a, c.$$

Similarly, by comparing $\mathcal{L}_2(\phi^\nu)$ with its linear part $\xi^2(\Delta + 1)^2 + 1$, we obtain

$$(B.3) \quad \xi^2(1 - \rho_j)^2 - M \leq \lambda_j^\nu \leq \xi^2(1 - \rho_j)^2 + M, \quad j = 1, 2, \dots, \quad \nu = a, c,$$

where the constant M is reused.

Denote

$$(B.4) \quad \tilde{R}_k^m = \prod_{j=k}^m \frac{\xi^2(1 - \rho_j)^2 + M}{\xi^2(1 - \rho_j)^2 - M},$$

and assume $\xi^2(1 - \rho_j)^2 - M > 0 \forall j > 0$ since otherwise we could start from the first positive term. Direct calculation shows that $\tilde{R}_4^\infty < +\infty$. With (B.3), we also know that the ratio R_4^∞ in (4.5) is well defined.

$\forall \epsilon_0 > 0$, there exists $N_0 > 0$ such that when $k, m > N_0$, we have $|R_4^k - R_4^m| < \epsilon_0$, and therefore $|R_4^k - R_4^\infty| \leq \epsilon_0$.

$1 < \tilde{R}_4^\infty < +\infty \implies$ there exists $N_1 > 0$ such that when $k, m > N_1$, we have

$$\tilde{R}_4^k \geq 1, \quad |\tilde{R}_4^k - \tilde{R}_4^m| < \epsilon_0,$$

and therefore $|\tilde{R}_4^k - \tilde{R}_4^\infty| \leq \epsilon_0$. Thus for $N_1 < k < m$, $|1 - \tilde{R}_{k+1}^m| = \frac{|\tilde{R}_4^k - \tilde{R}_4^m|}{|\tilde{R}_4^k|} < \epsilon_0$. Fixing $m_0 > \max\{N_0, N_1\}$ for $n > m_0$, we have

$$R_{4,\mathbf{n}}^n = R_{4,\mathbf{n}}^{m_0} R_{m_0+1,\mathbf{n}}^n \quad \text{and} \quad \lim_{n \rightarrow +\infty} R_{4,\mathbf{n}}^{m_0} = R_4^{m_0}$$

from (4.9). Hence there exists $\mathbf{n}_0 > (0, 0)$ such that $\forall \mathbf{n} > \mathbf{n}_0$, $n > m_0$, we have $|R_{4,\mathbf{n}}^{m_0} - R_4^\infty| < 2\epsilon_0$. Using (B.2), we have

$$(B.5) \quad 1 - \epsilon_0 < \frac{1}{1 + \epsilon_0} < (\tilde{R}_{m_0+1}^n)^{-1} \leq R_{m_0+1,\mathbf{n}}^n \leq \tilde{R}_{m_0+1}^n < 1 + \epsilon_0,$$

and thus

$$(B.6) \quad R_4^\infty + o(\epsilon_0) = (R_4^\infty - 2\epsilon_0)(1 - \epsilon_0) < R_{4,\mathbf{n}}^n < (R_4^\infty + 2\epsilon_0)(1 + \epsilon_0) = R_4^\infty + o(\epsilon_0).$$

Therefore we obtain the convergence. \square

REFERENCES

- [1] R. BARRY AND R. K. PACE, *Monte Carlo estimates of the log determinant of large sparse matrices*, Linear Algebra Appl., 289 (1999), pp. 41–54.
- [2] A. BESKOS, G. ROBERTS, A. M. STUART, AND J. VOSS, *MCMC methods for diffusion bridges*, Stoch. Dyn., 8 (2008), pp. 319–350.
- [3] P. M. CHAIKIN AND T. C. LUBENSKY, *Principles of Condensed Matter Physics*, Cambridge University Press, Cambridge, UK, 1997.
- [4] L. CHEN AND J. SHEN, *Application of semi-implicit Fourier spectral methods for phase field equations*, Comput. Phys. Comm., 108 (1998), pp. 147–158.
- [5] X. CHENG, L. LIN, W. E, P. ZHANG, AND A. SHI, *Nucleation of ordered phases in block copolymers*, Phys. Rev. Lett., 104 (2010), 148301.
- [6] M. DOI AND S. F. EDWARDS, *The Theory of Polymer Dynamics*, Internat. Ser. Monogr. Phys. 73, Oxford University Press, New York, 1986.
- [7] W. E, W. REN, AND E. VANDEN-EIJNDEN, *String method for the study of rare events*, Phys. Rev. B (3), 66 (2002), 052301.
- [8] W. E, W. REN, AND E. VANDEN-EIJNDEN, *Simplified and improved string method for computing the minimum energy paths in barrier-crossing events*, J. Chem. Phys., 126 (2007), 164103.
- [9] W. E AND E. VANDEN-EIJNDEN, *Transition-path theory and path-finding algorithms for the study of rare events*, Annu. Rev. Phys. Chem., 61 (2010), pp. 391–420.
- [10] W. E AND X. ZHOU, *The gentlest ascent dynamics*, Nonlinearity, 24 (2011), pp. 1831–1842.
- [11] P. C. FIFE, *Models for phase separation and their mathematics*, Electron. J. Differential Equations, no. 48 (2000).
- [12] G. H. FREDRICKSON, *The Equilibrium Theory of Inhomogeneous Polymers*, Internat. Ser. Monogr. Phys. 134, Oxford University Press, Oxford, UK, 2006.
- [13] I. W. HAMLEY, *The Physics of Block Copolymers*, Oxford University Press, Oxford, UK, 1998.
- [14] G. HENKELMAN AND H. JÓNSSON, *A dimer method for finding saddle points on high dimensional potential surfaces using only first derivatives*, J. Chem. Phys., 111 (1999), pp. 7010–7022.
- [15] G. HENKELMAN AND H. JÓNSSON, *Improved tangent estimate in the nudged elastic band method for finding minimum energy paths and saddle points*, J. Chem. Phys., 113 (2000), pp. 9978–9985.
- [16] T. W. HEO, L. ZHANG, Q. DU, AND L. CHEN, *Incorporating diffuse-interface nuclei in phase-field simulations*, Scripta Mater., 63 (2010), pp. 8–11.
- [17] P. C. HOHENBERG AND B. I. HALPERIN, *Theory of dynamic critical phenomena*, Rev. Modern Phys., 49 (1977), pp. 435–479.
- [18] C. JIN, W. REN, AND Y. XIANG, *Computing transition rates of thermally activated events in dislocation dynamics*, Scripta Mater., 62 (2010), pp. 206–209.
- [19] S. KOMURA, J. FUKUDA, AND G. C. PAQUETTE, *Interface dynamics in a block copolymer melt and the effect of noise*, Phys. Rev. E (3), 53 (1996), pp. R5588–R5591.
- [20] Y. LI AND J. ZHOU, *A local minimax method for finding multiple critical points and its applications to semilinear PDEs*, SIAM J. Sci. Comput., 23 (2001), pp. 840–865.

- [21] L. LIN, X. CHENG, W. E. A. SHI, AND P. ZHANG, *A numerical method for the study of nucleation of ordered phases*, J. Comput. Phys., 229 (2010), pp. 1797–1809.
- [22] M. W. MATSEN, *The standard Gaussian model for block copolymer melts*, J. Phys. Condens. Matter, 14 (2002), pp. R21–R47.
- [23] M. W. MATSEN AND M. SCHICK, *Stable and unstable phases of a diblock copolymer melt*, Phys. Rev. Lett., 72 (1994), pp. 2660–2663.
- [24] G. C. PAQUETTE, *Front propagation in a diblock copolymer melt*, Phys. Rev. A (3), 44 (1991), pp. 6577–6599.
- [25] G. DA PRATO AND A. DEBUSSCHE, *Stochastic Cahn-Hilliard equation*, Nonlinear Anal., 26 (1996), pp. 241–263.
- [26] G. DA PRATO AND J. ZABCZYK, *Stochastic Equations in Infinite Dimensions*, Cambridge University Press, Cambridge, UK, 1992.
- [27] T. QIAN, W. REN, AND P. SHENG, *Current dissipation in thin superconducting wires: A numerical evaluation using the string method*, Phys. Rev. B (3), 72 (2005), 014512.
- [28] A. SHI AND J. NOOLANDI, *Nature of anisotropic fluctuation modes in ordered polymeric phases*, Polymer, 39 (1998), pp. 4649–4654.
- [29] G. STRANG AND G. FIX, *An Analysis of the Finite Element Method*, 2nd ed., Wellesley-Cambridge Press, Wellesley, MA, 2008.
- [30] E. VANDEN-ELJNDEN AND M. G. WESTDICKENBERG, *Rare events in stochastic partial differential equations on large spatial domains*, J. Stat. Phys., 131 (2008), pp. 1023–1038.
- [31] R. A. WICKHAM, A. SHI, AND Z. WANG, *Nucleation of stable cylinders from a metastable lamellar phase in a diblock copolymer melt*, J. Chem. Phys., 118 (2003), pp. 10293–10305.
- [32] L. ZHANG, L. CHEN, AND Q. DU, *Morphology of critical nuclei in solid-state phase transformations*, Phys. Rev. Lett., 98 (2007), 265703.
- [33] P. ZHANG AND X. ZHANG, *An efficient numerical method of Landau-Brazovskii model*, J. Comput. Phys., 227 (2008), pp. 5859–5870.
- [34] W. ZHANG, T. LI, AND P. ZHANG, *Numerical study for the nucleation of one-dimensional stochastic Cahn-Hilliard dynamics*, Commun. Math. Sci., 10 (2012), pp. 1105–1132.
- [35] Y. ZHANG AND W. E. LEITHEAD, *Approximate implementation of logarithm of the matrix determinant in Gaussian process regression*, J. Statist. Comput. Simul., 77 (2007), pp. 329–348.